Comparison of high-order Eulerian methods for electron hybrid model

Anaïs Crestetto[a], Nicolas Crouseilles[b], Yingzhe Li[c], and Josselin Massot[d]

[a]Université de Nantes, LMJL, UMR 6629, France
[b]Univ Rennes, Inria Bretagne Atlantique (MINGuS) & IRMAR UMR 6625 & ENS Rennes, France
[c]Max Planck Institute for Plasma Physics, Boltzmannstrasse 2, 85748 Garching, Germany
[d]Univ Rennes, IRMAR UMR 6625 & Inria Bretagne Atlantique (MINGuS), France

Contents

Abstract

In this work, we focus on the numerical approximation of a hybrid fluid-kinetic plasma model for electrons, in which energetic electrons are described by a Vlasov kinetic model whereas a fluid model is used for the cold population of electrons. First, we study the validity of this hybrid modelling in a two dimensional context (one dimension in space and one dimension in velocity) against the full (stiff) Vlasov kinetic model and second, a four dimensional configuration is considered (one dimension in space and three dimensions in velocity) following [1]. To do so, we consider two numerical Eulerian methods. The first one is based on the Hamiltonian structure of the hybrid system and the second approach, which is based on exponential integrators, enables to derive high order integrator and remove the CFL condition induced by the linear part. The efficiency of these methods, which are combined with an adaptive time stepping strategy, are discussed in the different configurations and in the linear and nonlinear regimes.

1 Introduction

The goal of this work is to numerically solve hybrid fluid-kinetic models describing charged particles systems in which hot particles interact with a cold bulk. Such a configuration can be studied in tokamak plasmas where alpha-particles (generated by fusion reaction) interact with the plasma. Another example can be found in the atmosphere where suprathermal electrons of solar wind interact with Earth magnetosphere. Due to the strong thermal velocity ratio between cold and hot particles, the original kinetic model is too costly from a numerical point of view, in particular because the velocity mesh has to be very fine to capture the thermal velocity of cold particles. Thus, the derivation of simplified model is of great interest. Specific models have been proposed in such context (see [1],[2],[3],[4],[5],[6]) which are derived from a reference kinetic description for the whole plasma. A distribution function is then introduced for the electrons: $f(t, x, v) \in \mathbb{R}_+$ is the solution of a Vlasov-Maxwell system (ions are supposed fixed). Assuming the electrons population can be split into a cold population f_c and a population of energetic (hot) electrons f_h, a first step, consists in decomposing the original

distribution function f as $f = f_c + f_h$. This decomposition let us solve the thermal velocity ratio problem since kinetic functions f_c and f_h could be solved on distinct velocity meshes. However we can go further to remove velocity mesh on f_c. Indeed in a second step, it is assumed that the cold particles are close to a thermodynamical equilibrium with a temperature $T_c \ll 1$ and as such can be approximated by a fluid model. A hybrid fluid-kinetic model is then obtained which can be simplified again by neglecting nonlinear terms of the cold (fluid) part (the wave perturbation of cold particles have small amplitude). The so-obtained model is called Vlasov-Hybrid linearized (VHL) (see [1]) and it is the goal of this work to check its validity compared to the original full kinetic model and to propose new specific numerical methods for its discretization.

To numerically solve the VHL model, we propose here two methods. The first one lies on the fact that the VHL model has a noncanonical Hamiltonian structure [8],[5],[6], which ensures the preservation of invariants like the total energy. The objectif is to exploit this structure to construct numerical schemes which will have a good long time behavior [9],[10],[11],[12],[13]. The first scheme is a splitting scheme designed from a *splitting* of the Hamiltonian. This approach enables to combine in a clever way the terms of the model and we are led to solve simple subsystems (like in [12],[14],[10]). A remarkable property is that each subsystem can be solved exactly in time, the error in time thus only comes from the splitting method, knowing that splitting methods of arbitrary order can be derived by composition ([13]). The second method belongs to the family of exponential and Lawson integrators [15],[16],[17],[18],[19],[20]. Indeed, exploiting the fact that the linear part of the VHL model can be solved exactly and efficiently, high order Lawson schemes are constructed. We mention that these two methods (splitting and Lawson) can be combined with adaptive time stepping strategies. For Lawson methods, we benefit from the framework of embedded methods [21],[22],[23],[24] for which the local error can be computed easily. For the splitting methods, the recent work [25] gives alternative strategies which enable us to compare these techniques in the charged particles context. Note that for the phase space approximation, spectral methods are used in space whereas high order finite difference methods (WENO) are used in velocity.

The Hamiltonian splitting bears similarities with the approaches proposed by [11] or [1]. However, in these papers, Particle-In-Cell methods are used in phase-space whereas Eulerian methods are used in the present work. Thus, this work is closer to the papers [12],[10] in which an operator splitting is performed before discretizing, whereas in [11] and [1], a phase-space discretization is performed before discretizing in time.

To validate our numerical methods, we use relation dispersion to compute the instability rates. We can go further by reconstructing the fundamental mode of the electric field (see [26],[27]). In addition to precise way to validate the codes, this study enables to make the link between the models (full kinetic and VHL).

The rest of the paper is organized as follows. First the VHL model and its Hamiltonian structure are presented. Then, the two time discretizations (Hamiltonian splitting and Lawson) are introduced. In Section 4, we focus on the 1dx-1dv case in which we discuss the domain of validity of the VHL with respect the the full kinetic model. Finally, Section 5 is dedicated to the 1dx-3dv case.

2 Electron hybrid model

Following [1], we consider a hybrid system for which the electron population mainly consists of cold electrons (the unknown will be denoted with a subscript "c") which are approximated by a thermal equilibrium with zero temperature (the so-called cold plasma approximation). Its kinetic description can be seen as a Dirac mass, limit of a Gaussian function as the temperature T_c goes to zero:

$$f_c(t,\mathbf{x},\mathbf{v}) = \rho_c(t,\mathbf{x})\delta_{\mathbf{v}=\mathbf{u}_c(t,\mathbf{x})}(\mathbf{v}) = \lim_{T_c\to 0} \frac{\rho_c(t,\mathbf{x})}{(2\pi T_c(t,\mathbf{x}))^{3/2}} \exp\left(-\frac{|\mathbf{v}-\mathbf{u}_c(t,\mathbf{x})|^2}{2T_c(t,\mathbf{x})}\right). \quad (1)$$

Moreover, a small amount of energetic electrons (the unknown will be denoted with a subscript "h") is considered, through a kinetic description. The ions are supposed to form a stationary background of density ρ_i. Based on these assumptions, a hybrid fluid-kinetic model is considered for the cold and hot populations, coupled with Maxwell equation for the electromagnetic field. Indeed, from the full electron Vlasov-Maxwell system satisfied by the distribution function $f(t,\mathbf{x},\mathbf{v})$ with the time $t \geq 0$, the space $\mathbf{x} \in \Omega \subset \mathbb{R}^3$ and the velocity $\mathbf{v} \in \mathbb{R}^3$), $\mathbf{B}_0 \in \mathbb{R}^3$ being an external magnetic field, which writes

$$\begin{aligned}
\frac{\partial f}{\partial t} &+ \mathbf{v}\cdot\nabla f + \frac{q_e}{m_e}\left(\mathbf{E}+\mathbf{v}\times(\mathbf{B}+\mathbf{B}_0)\right)\cdot\nabla_{\mathbf{v}} f = 0,\\
\frac{\partial \mathbf{B}}{\partial t} &= -\nabla\times\mathbf{E},\\
\frac{1}{c^2}\frac{\partial \mathbf{E}}{\partial t} &= \nabla\times\mathbf{B} - \mu_0 q_e \int_{\mathbb{R}^3} \mathbf{v} f \mathrm{d}\mathbf{v},\\
\nabla\cdot\mathbf{E} &= \frac{1}{\varepsilon_0}\left[q_i\rho_i + q_e\int_{\mathbb{R}^3} f\mathrm{d}\mathbf{v}\right],\\
\nabla\cdot\mathbf{B} &= 0,
\end{aligned}$$

the decomposition $f(t,\mathbf{x},\mathbf{v}) = f_c(t,\mathbf{x},\mathbf{v}) + f_h(t,\mathbf{x},\mathbf{v})$ together with the approximation (2) leads to the following fluid-kinetic hybrid model

$$\begin{aligned}
\frac{\partial \rho_c}{\partial t} &+ \nabla\cdot(\rho_c\mathbf{u}_c) = 0,\\
\frac{\partial(\rho_c\mathbf{u}_c)}{\partial t} &+ \nabla\cdot(\rho_c\mathbf{u}_c\otimes\mathbf{u}_c) = \frac{q_e\rho_c}{m_e}(\mathbf{E}+\mathbf{u}_c\times(\mathbf{B}+\mathbf{B}_0)),\\
\frac{\partial f_h}{\partial t} &+ \mathbf{v}\cdot\nabla f_h + \frac{q_e}{m_e}\left(\mathbf{E}+\mathbf{v}\times(\mathbf{B}+\mathbf{B}_0)\right)\cdot\nabla_{\mathbf{v}} f_h = 0,\\
\frac{\partial \mathbf{B}}{\partial t} &= -\nabla\times\mathbf{E},\\
\frac{1}{c^2}\frac{\partial \mathbf{E}}{\partial t} &= \nabla\times\mathbf{B} - \mu_0(\mathbf{j}_c+\mathbf{j}_h),\\
\nabla\cdot\mathbf{E} &= \frac{1}{\varepsilon_0}[q_i\rho_i + q_e(\rho_c+\rho_h)],\\
\nabla\cdot\mathbf{B} &= 0,\\
\mathbf{j}_c &= q_e\rho_c\mathbf{u}_c,\\
\mathbf{j}_h &= q_e\int_{\mathbb{R}^3}\mathbf{v} f_h \mathrm{d}\mathbf{v} := q_e\rho_h\mathbf{u}_h,
\end{aligned}$$

where the moments of the hot particles are denoted by

$$\int_{\mathbb{R}^3} (1, \mathbf{v}) f_h \, \mathrm{d}\mathbf{v} = (\rho_h, \rho_h \mathbf{u}_h).$$

Initial and boundary conditions which are necessary to complete the model will be given below.

The above hybrid model can be reduced to an equivalent set of equations for the unknown $(\mathbf{u}_c, \mathbf{B}, \mathbf{E}, f_h)$, or equivalently $(\mathbf{j}_c, \mathbf{B}, \mathbf{E}, f_h)$, which we intend to solve numerically. This derivation is detailed in [1] and we refer the reader to this work. We then write

$$\begin{aligned}
&\frac{\partial \mathbf{j}_c}{\partial t} + \nabla \cdot \left(\mathbf{j}_c \otimes \frac{\mathbf{j}_c}{q_e \rho_c} \right) = \frac{q_e}{m_e} (q_e \rho_c \mathbf{E} + \mathbf{j}_c \times (\mathbf{B} + \mathbf{B}_0)), \\
&\frac{\partial f_h}{\partial t} + \mathbf{v} \cdot \nabla f_h + \frac{q_e}{m_e} (\mathbf{E} + \mathbf{v} \times (\mathbf{B} + \mathbf{B}_0)) \cdot \nabla_{\mathbf{v}} f_h = 0, \\
&\frac{\partial \mathbf{B}}{\partial t} = -\nabla \times \mathbf{E}, \\
&\frac{1}{c^2} \frac{\partial \mathbf{E}}{\partial t} = \nabla \times \mathbf{B} - \mu_0 (\mathbf{j}_c + \mathbf{j}_h).
\end{aligned}$$

Still following [1], the system is further simplified by considering a linearization of the equations around a stationary state $(\rho_c = \rho_c^{(0)}(\mathbf{x}), \mathbf{j}_c = \mathbf{0}, \mathbf{B} = \mathbf{B}_0(\mathbf{x}), \mathbf{E} = \mathbf{0}, f_h = f_h^0(\mathbf{x}, \mathbf{v}))$. We finally get the following system satisfied by the perturbation (the same notation as before are however kept)

$$\frac{\partial \mathbf{j}_c}{\partial t} = \varepsilon_0 \Omega_{pe}^2 \mathbf{E} + \mathbf{j}_c \times \frac{q_e}{m_e} \mathbf{B}_0(\mathbf{x}), \tag{2}$$

$$\frac{\partial f_h}{\partial t} + \mathbf{v} \cdot \nabla f_h + \frac{q_e}{m_e} (\mathbf{E} + \mathbf{v} \times (\mathbf{B} + \mathbf{B}_0)) \cdot \nabla_{\mathbf{v}} f_h = 0, \tag{3}$$

$$\frac{\partial \mathbf{B}}{\partial t} = -\nabla \times \mathbf{E}, \tag{4}$$

$$\frac{1}{c^2} \frac{\partial \mathbf{E}}{\partial t} = \nabla \times \mathbf{B} - \mu_0 \mathbf{j}_c - \mu_0 q_e \int_{\mathbb{R}^3} \mathbf{v} f_h \, \mathrm{d}\mathbf{v}, \tag{5}$$

where $\Omega_{pe}^2(\mathbf{x}) = q_e^2 \rho_c^{(0)}(\mathbf{x}) / (\varepsilon_0 m_e)$.

Let us remark that will be possible to consider a Maxwellian closure instead of the Dirac closure . It will enrich the nonlinear part, but here we chose to consider model proposed in [1].

The energy (Hamiltonian) is

$$\mathcal{H} = \underbrace{\frac{\varepsilon_0}{2} \int_\Omega |\mathbf{E}|^2 \mathrm{d}\mathbf{x}}_{\mathcal{H}_E} + \underbrace{\frac{1}{2\mu_0} \int_\Omega |\mathbf{B}|^2 \mathrm{d}\mathbf{x}}_{\mathcal{H}_B} + \underbrace{\frac{1}{2\varepsilon_0} \int_\Omega \frac{1}{\Omega_{pe}^2} |\mathbf{j}_c|^2 \mathrm{d}\mathbf{x}}_{\mathcal{H}_{j_c}} + \underbrace{\frac{m_e}{2} \int_\Omega \int_{\mathbb{R}^3} |\mathbf{v}|^2 f_h \, \mathrm{d}\mathbf{x} \mathrm{d}\mathbf{v}}_{\mathcal{H}_{f_h}}. \tag{6}$$

According to [5], the linearized hybrid model possesses a noncanonical structure. It is always a difficult issue to determine the bracket of a Hamiltonian system and thus to exhibit a canonical structure. Here, we define for the first time a bracket for the linear

hybrid model. For two given functionals $\mathcal{F}, \mathcal{G}$ of $\mathbf{j}_c, \mathbf{B}, \mathbf{E}, f_h$, the Poisson bracket is given by

$$\begin{aligned}
\{\mathcal{F},\mathcal{G}\}[\mathbf{j}_c,\mathbf{B},\mathbf{E},f_h] = & \frac{1}{m_e}\int_\Omega\int_{\mathbb{R}^3} f_h\Big[\frac{\delta\mathcal{F}}{\delta f_h},\frac{\delta\mathcal{G}}{\delta f_h}\Big]_{\mathbf{xv}}\mathrm{d}\mathbf{v}\mathrm{d}\mathbf{x}\\
&+\frac{q_e}{m_e\varepsilon_0}\int_\Omega\int_{\mathbb{R}^3} f_h\left(\nabla_{\mathbf{v}}\frac{\delta\mathcal{F}}{\delta f_h}\cdot\frac{\delta\mathcal{G}}{\delta\mathbf{E}}-\nabla_{\mathbf{v}}\frac{\delta\mathcal{G}}{\delta f_h}\cdot\frac{\delta\mathcal{F}}{\delta\mathbf{E}}\right)\mathrm{d}\mathbf{v}\mathrm{d}\mathbf{x}\\
&+\frac{q_e}{m_e^2}\int_\Omega\int_{\mathbb{R}^3} f_h(\mathbf{B}+\mathbf{B}_0)\cdot\left(\nabla_{\mathbf{v}}\frac{\delta\mathcal{F}}{\delta f_h}\times\nabla_{\mathbf{v}}\frac{\delta\mathcal{G}}{\delta f_h}\right)\mathrm{d}\mathbf{v}\mathrm{d}\mathbf{x}\\
&+\frac{1}{\varepsilon_0}\int_\Omega\left(\nabla\times\frac{\delta\mathcal{F}}{\delta\mathbf{E}}\cdot\frac{\delta\mathcal{G}}{\delta\mathbf{B}}-\nabla\times\frac{\delta\mathcal{G}}{\delta\mathbf{E}}\cdot\frac{\delta\mathcal{F}}{\delta\mathbf{B}}\right)\mathrm{d}\mathbf{x}\\
&+\int_\Omega\Omega_{pe}^2\left(\frac{\delta\mathcal{F}}{\delta\mathbf{j}_c}\cdot\frac{\delta\mathcal{G}}{\delta\mathbf{E}}-\frac{\delta\mathcal{G}}{\delta\mathbf{j}_c}\cdot\frac{\delta\mathcal{F}}{\delta\mathbf{E}}\right)\mathrm{d}\mathbf{x}\\
&+\frac{q_e\varepsilon_0}{m_e}\int_\Omega\Omega_{pe}^2\mathbf{B}_0\cdot\left(\frac{\delta\mathcal{F}}{\delta\mathbf{j}_c}\times\frac{\delta\mathcal{G}}{\delta\mathbf{j}_c}\right)\mathrm{d}\mathbf{x}. \qquad (7)
\end{aligned}$$

The two last terms are new compared with the Poisson bracket of Vlasov–Maxwell equations. The following theorem ensures that the above bracket is indeed a Poisson bracket (the proof is given in appendix A).

Theorem 2.1. *The above bracket defined by (7) is a Poisson bracket.*

From this result, we can reformulate the hybrid model as

$$\partial_t U = \{U, \mathcal{H}\}, \qquad (8)$$

where $\mathcal{H}$ denotes the Hamiltonian (6), $U = (\mathbf{j}_c, \mathbf{B}, \mathbf{E}, f_h)$, and $\{\cdot,\cdot\}$ the bracket defined in (7).

In the next sections, we consider dimensionless quantities. The derivation of dimensionless equations is given in Appendices B and C according to the dimension of the phase space.

3 Time discretizations

In this section, we succinctly present two time discretizations for the hybrid model which will be developed in the $1dx - 1dv$ and $1dx - 3dv$ case. Regarding the Hamiltonian structure, we will use a Hamiltonian splitting which is particularly well suited in our case. Moreover, the linearization of the fluid part makes the use of exponential methods very attractive in this context as well. Our goal will be to compare the efficiency of these two integrators.

3.1 Hamiltonian splitting

From the previous section, we derive a time splitting to numerically solve (2)-(5), in its dimensionless form (see Appendix B). Indeed, we can reformulate the hybrid model as

(8), where $\mathcal{H}$ denotes the Hamiltonian (6), U is a functional of the unknown $(\mathbf{j}_c, \mathbf{B}, \mathbf{E}, f_h)$, and $\{\cdot,\cdot\}$ is the bracket defined in (7). We construct the splitting from the decomposition of the Hamiltonian $\mathcal{H} = \mathcal{H}_{\mathbf{E}} + \mathcal{H}_{\mathbf{B}} + \mathcal{H}_{\mathbf{j}_c} + \mathcal{H}_{f_h}$ so that the following equation

$$\frac{\partial U}{\partial t} = \{U, \mathcal{H}_{\mathbf{E}}\} + \{U, \mathcal{H}_{\mathbf{B}}\} + \{U, \mathcal{H}_{\mathbf{j}_c}\} + \{U, \mathcal{H}_{f_h}\}$$

can be split into 4 subsystems which will be written down in the following.

Equations for $\mathcal{H}_{\mathbf{E}}$

We derive here the equations corresponding to $\partial_t U = \{U, \mathcal{H}_{\mathbf{E}}\}$, for $U = (\mathbf{j}_c, \mathbf{B}, \mathbf{E}, f_h)$ and with $\mathcal{H}_{\mathbf{E}} = \frac{1}{2}\int_\Omega |\mathbf{E}|^2 \mathrm{d}\mathbf{x}$. From the following relations

$$\frac{\delta \mathcal{H}_{\mathbf{E}}}{\delta f_h} = \frac{\delta \mathcal{H}_{\mathbf{E}}}{\delta \mathbf{B}} = \frac{\delta \mathcal{H}_{\mathbf{E}}}{\delta \mathbf{j}_c} = 0, \quad \text{and} \quad \frac{\delta \mathcal{H}_{\mathbf{E}}}{\delta \mathbf{E}} = \mathbf{E},$$

the first step of the splitting gives for f_h

$$\partial_t f_h \;=\; \mathbf{E} \cdot \nabla_v f_h,$$

and for $\mathbf{E}, \mathbf{B}, \mathbf{j}_c$, we obtain

$$\partial_t \mathbf{E} = 0, \;\; \partial_t \mathbf{B} = -\nabla \times \mathbf{E}, \;\; \partial_t \mathbf{j}_c = \Omega_{pe}^2 \mathbf{E}.$$

Let us remark that this system can be solved exactly in time.

Equations for $\mathcal{H}_{\mathbf{B}}$

We derive here the equations corresponding to $\partial_t U = \{U, \mathcal{H}_{\mathbf{B}}\}$, for $U = (\mathbf{j}_c, \mathbf{B}, \mathbf{E}, f_h)$. We obtain

$$\partial_t f_h = 0, \;\; \partial_t \mathbf{E} = \nabla \times \mathbf{B}, \;\; \partial_t \mathbf{B} = 0, \partial_t \mathbf{j}_c = 0,$$

which can be solved exactly in time.

Equations for $\mathcal{H}_{\mathbf{j}_c}$

We derive here the equations corresponding to $\partial_t U = \{U, \mathcal{H}_{\mathbf{j}_c}\}$, for $U = (\mathbf{j}_c, \mathbf{B}, \mathbf{E}, f_h)$. We obtain

$$\partial_t f_h = 0, \;\; \partial_t \mathbf{E} = -\mathbf{j}_c, \;\; \partial_t \mathbf{B} = 0, \;\; \partial_t \mathbf{j}_c = -\mathbf{j}_c \times \mathbf{B}_0,$$

which can be solved exactly in time.

Equations for $\mathcal{H}_{f_h}$

We derive here the equations corresponding to $\partial_t U = \{U, \mathcal{H}_{f_h}\}$, for $U = (\mathbf{j}_c, \mathbf{B}, \mathbf{E}, f_h)$. We obtain

$$\begin{aligned} \partial_t f_h &= -\mathbf{v} \cdot \nabla f_h + (\mathbf{v} \times (\mathbf{B} + \mathbf{B}_0)) \cdot \nabla_{\mathbf{v}} f_h, \\ \partial_t \mathbf{E} &= \int \mathbf{v} f_h \, \mathrm{d}\mathbf{v}, \partial_t \mathbf{B} = 0, \quad \partial_t \mathbf{j}_c = 0. \end{aligned}$$

This system can *not* be solved exactly in time. However, we can split again the term $\mathcal{H}_{f_h}$ as follows

$$\mathcal{H}_{f_h} := \frac{1}{2}\int |\mathbf{v}|^2 f_h \,\mathrm{d}\mathbf{v} = \frac{1}{2}\int v_x^2 f_h \,\mathrm{d}\mathbf{v} + \frac{1}{2}\int v_y^2 f_h \,\mathrm{d}\mathbf{v} + \frac{1}{2}\int v_z^2 f_h \,\mathrm{d}\mathbf{v} =: \mathcal{H}_{f_{h,x}} + \mathcal{H}_{f_{h,y}} + \mathcal{H}_{f_{h,z}}.$$

Then, we get for $\mathcal{H}_{f_{h,\star}}$, with symbol $\star \in \{x, y, z\}$,

$$\partial_t f_h = -v_\star \partial_\star f_h + \sum_{j\in\{x,y,z\}} \hat{B}_{j,\star} v_\star \partial_{v_j} f_h, \quad \partial_t \mathbf{E} = \int v_\star f_h \,\mathrm{d}\mathbf{v},$$

where we denote $\hat{\mathbf{B}}$ the traceless matrix such that $\mathbf{v}\times(\mathbf{B}+\mathbf{B}_0) := \hat{\mathbf{B}}\mathbf{v}$. It turns out that this system can be solved exactly in time (see [9] and below for more details).

Hence, denoting $\varphi_t^{[E]}, \varphi_t^{[B]}, \varphi_t^{[j_c]}, \varphi_t^{[f_h]}$ the respective solutions of the previous subsystems, for a given initial condition $U(t=0) = U_0 = (\mathbf{j}_c(0), \mathbf{B}(0), \mathbf{E}(0), f_h(0))$, the solution $\varphi_t(U_0)$ of the whole system at time t is approximated by the so-called Lie-Trotter splitting

$$\varphi_t(U_0) \approx \varphi_t^{[E]} \circ \varphi_t^{[B]} \circ \varphi_t^{[j_c]} \circ \varphi_t^{[f_h]}(U_0). \tag{9}$$

Now denoting U^n a time approximation of U at time $t_n = n\Delta t$, $n \in \mathbb{N}$, $\Delta t > 0$ being the time step, high order splittings can be constructed from the decomposition (9). We will use the so-called Suzuki method [28] which can be constructed from the Strang splitting basic block [29] whose formulation reads

$$U^{n+1} = S_{\Delta t}(U^n) = \varphi^{[E]}_{\Delta t/2} \circ \varphi^{[j_c]}_{\Delta t/2} \circ \varphi^{[B]}_{\Delta t/2} \circ \varphi^{[f_h]}_{\Delta t} \circ \varphi^{[B]}_{\Delta t/2} \circ \varphi^{[j_c]}_{\Delta t/2} \circ \varphi^{[E]}_{\Delta t/2}(U^n), \tag{10}$$

where the most costly step $\varphi^{[f_h]}_{\Delta t}$ has been put in the middle to be evaluated only once per time step. The Suzuki method can be written as a composition of 5 Strang methods (which leads to 25 stages):

$$U^{n+1} = \mathcal{S}_{\Delta t}(U^n) = S_{\alpha_1\Delta t} \circ S_{\alpha_2\Delta t} \circ S_{\alpha_3\Delta t} \circ S_{\alpha_2\Delta t} \circ S_{\alpha_1\Delta t}(U^n), \tag{11}$$

where the constants α_i are defined by

$$\alpha_1 = \alpha_2 = \frac{1}{4 - \sqrt[3]{4}}, \qquad \alpha_3 = \frac{1}{1 - 4^{\frac{2}{3}}}. \tag{12}$$

Let us recall that the Strang method is second order accurate whereas the Suzuki method is fourth order. We refer to [30] for other composition methods designed from a three terms decomposition. We observe that the number of stages increases dramatically when high order are considered which is, as we will see, a drawback of these methods.

3.2 Lawson methods

The VHL system (2)-(5) (in its dimensionless form proposed in Appendix B), can be rewritten by splitting the linear part and the nonlinear part as

$$\partial_t U + AU + N(t, U) = 0,$$

where $U(t,\mathbf{x},\mathbf{v}) = (\mathbf{j}_c(t,\mathbf{x}), \mathbf{B}(t,\mathbf{x}), \mathbf{E}(t,\mathbf{x}), f_h(t,\mathbf{x},\mathbf{v}))^{\mathsf{T}}$, A is a 10x10 matrix and N is a function to be defined. If all the linear terms are taken into account, the linear part A reads

$$AU = \begin{pmatrix} \hat{\mathbf{B}}_0 & \mathbf{0}_3 & -\Omega_{pe}^2\mathbf{I}_3 & \tilde{0}^T \\ \mathbf{0}_3 & \mathbf{0}_3 & \hat{\nabla} & \tilde{0}^T \\ \mathbf{I}_3 & -\hat{\nabla} & \mathbf{0}_3 & \tilde{0}^T \\ \tilde{0} & \tilde{0} & \tilde{0} & \mathcal{L} \end{pmatrix} U, \tag{13}$$

where $\hat{\nabla}$ is defined such that $\nabla \times \mathbf{u} = \hat{\nabla}\mathbf{u}$ for all function $\mathbf{u} \in \mathbb{R}^3$, $\mathbf{0}_3$ is a 3x3 matrix with 0 entries, $\mathcal{L} := \mathbf{v}\cdot\nabla - (\mathbf{v}\times\mathbf{B}_0)\cdot\nabla_{\mathbf{v}}$, with $\hat{\mathbf{B}}_0$ the 3x3 matrix such that $\mathbf{j}_c \times \mathbf{B}_0 = \hat{\mathbf{B}}_0\mathbf{j}_c$, $\tilde{0} = (0,0,0)$, and the nonlinear part reads

$$N(t,U) = \begin{pmatrix} \tilde{0}^T \\ \tilde{0}^T \\ -\int_{\mathbb{R}^3} \mathbf{v} f_h \,\mathrm{d}\mathbf{v} \\ -(\mathbf{E} + \mathbf{v}\times\mathbf{B})\cdot\nabla_{\mathbf{v}} f_h \end{pmatrix}.$$

In fact term $\int_{\mathbb{R}^3} \mathbf{v} f_h \,\mathrm{d}\mathbf{v}$ is linear in f_h, but non local. We decide to consider it explicitly in the nonlinear term to avoid an increase of the size of A and U. Once the VHL system has been reformulated this way, exponential and Lawson integrators can be used. Following [20], we shall use Lawson integrators for stability reasons. The basics of the Lawson schemes are reminded in the following. In a first step, the linear part is filtered out by considering $V(t) = e^{tA}U$ so that we get

$$\partial_t V + \tilde{N}(t,V) = 0 \tag{14}$$

with $\tilde{N} : (t,V) \mapsto e^{tA}N(t, e^{-tA}V)$. Then, in a second step, a Runge-Kutta method is used for (14) which can be reformulated into a numerical method on U (see [17]). Considering only explicit Runge-Kutta methods with s-stages, the Butcher tableau reads

$$\begin{array}{c|cccc} 0 & & & & \\ c_2 & a_{2,1} & & & \\ \vdots & \vdots & \ddots & & \\ c_s & a_{s,1} & \cdots & a_{s,s-1} & \\ \hline & b_1 & \cdots & b_{s-1} & b_s \end{array}$$

so that the numerical scheme for (14) is

$$V^{(i)} = V^n - \Delta t \sum_{j=1}^{i-1} a_{ij} \tilde{N}(t_n + c_j\Delta t, V^{(j)}), \quad i = 1,\ldots,s,$$

$$V^{n+1} = V^n - \Delta t \sum_{i=1}^{s} b_i \tilde{N}(t_n + c_i\Delta t, V^{(i)}),$$

and in a last step, we come back to the unknown U to get

$$U^{(i)} = e^{-c_i \Delta t A} U^n - \Delta t \sum_{j=1}^{i-1} a_{i,j} e^{(c_j - c_i)\Delta t A} N(t_n + c_j \Delta t, U^{(j)}), \quad i = 1, \dots, s,$$

$$U^{n+1} = e^{-\Delta t A} U^n - \Delta t \sum_{i=1}^{s} b_i e^{(c_i - 1)\Delta t A} N(t_n + c_i \Delta t, U^{(i)}).$$

As we shall see in the next sections, the efficiency of Lawson integrators is strongly related to the cost of the evaluation of $\exp(A)$. It turns out that in the $1dx - 3dv$ case, the evaluation of $\exp(A)$ is very expensive if not impossible, even using formal languages. Thus, one strategy may be to transfer some terms from the linear part to the nonlinear part making the calculation of $\exp(A)$ doable, still leading to efficient schemes.

3.3 Adaptive time step methods

We end this numerical section by discussing the possibility to use adaptive time step strategies. For the two integrators presented before, we will see that adaptive time step methods can be incorporated. This can be of great interest in many applications, in particular in plasma physics for which a linear phase can be solved using large time steps whereas for the nonlinear phase, which involves strong gradients and small time scales, small time steps may be preferred to capture important physical phenomena (see [20]).

To remind the basics of the adaptive time stepping strategy, we consider an ODE satisfied by $U(t) \in \mathbb{R}^d$. Basically, adaptive time stepping requires two numerical solutions at time t_{n+1} computed with two different integrators of different orders. Typically, we will denote $U^{n+1}_{[p]}$ (resp. $U^{n+1}_{[p+1]}$) the numerical solution computed with an integrator of order p (resp. $p+1$)

$$U^{n+1}_{[p]} = U(t_{n+1}) + \mathcal{O}((\Delta t_n)^{p+1}) \qquad U^{n+1}_{[p+1]} = U(t_{n+1}) + \mathcal{O}((\Delta t_n)^{p+2}),$$

where Δt_n is the time step used at iteration n to compute $U^{n+1}_{[p]}$ and $U^{n+1}_{[p+1]}$. Combining these two solutions enables to estimate the local error on the solution of lower order

$$L^{n+1}_{[p]} = \| U^{n+1}_{[p+1]} - U^{n+1}_{[p]} \| \tag{15}$$

(here $\| \cdot \|$ is a vectorial norm to be defined according to the problem), and to compute the time step for the next iteration

$$\Delta t_{n+1} = \sqrt[p]{\frac{\text{tol}}{L^{n+1}_{[p]}}} \Delta t_n, \tag{16}$$

with the user-specified tolerance tol. Thus, there are two situations: (i) if the local error $L^{n+1}_{[p]}$ is larger than the user-specified tolerance tol, the iteration is *rejected* and is restarted by recomputing $U^{n+1}_{[p]}$ with a smaller time step given by (16). (ii) otherwise, if the local error $L^{n+1}_{[p]}$ is smaller than tol, $U^{n+1}_{[p]}$ is kept as approximated solution at time t_{n+1} and a new time step is computed according to (16), which ensures that the local error at the former time will be smaller than tol.

Adaptive time step method for the Hamiltonian splitting method

We incorporate adaptive time stepping strategies in the Hamiltonian splitting presented in Subsection 3.1, following the recent work [25]. We choose the Suzuki splitting (11) and define the substep solution $U^{(m)}$, $m = 1, \dots, 4$, as follows

$$U_{[4]}^{n+1} = \mathcal{S}_{\Delta t}(U^n) = S_{\alpha_1\Delta t} \circ S_{\alpha_2\Delta t} \circ S_{\alpha_3\Delta t} \circ S_{\alpha_2\Delta t} \circ \underbrace{S_{\alpha_1\Delta t}(U^n)}_{U^{(1)}}.$$
$$\underbrace{\qquad\qquad\qquad\qquad\qquad\qquad}_{U^{(2)}}$$
$$\underbrace{\qquad\qquad\qquad\qquad\qquad\qquad\qquad\qquad}_{U^{(3)}}$$
$$\underbrace{\qquad\qquad\qquad\qquad\qquad\qquad\qquad\qquad\qquad\qquad}_{U^{(4)}}$$

The advantage of this approach introduced in [25] comes from the fact that the lower order integrator uses a linear combination of the outputs generated by the intermediate steps of the splitting. Then, as soon as the number of stages is large enough, low order integrator can be designed and the strategy is cost-free. Using a linear combination of $\left(U^{(m)}\right)_{m\in[\![1,4]\!]}$, where $U^{(1)} = S_{\alpha_1\Delta t}(U^n)$, $U^{(2)} = S_{\alpha_2\Delta t}(U^{(1)})$, $U^{(3)} = S_{\alpha_3\Delta t}(U^{(2)})$, $U^{(4)} = S_{\alpha_2\Delta t}(U^{(3)})$, a third order approximation of $U(t^{n+1})$ can be obtained

$$U_{[3]}^{n+1} = -U_{[4]}^{n} + w_1(U^{(1)} + U^{(4)}) + w_2(U^{(2)} + U^{(3)})$$

with

$$w_1 = \frac{g_2(1-g_2)}{g_1(g_1-1) - g_2(g_2-1)}, \qquad w_2 = 1 - w_1$$

and $g_1 = \alpha_1$, $g_2 = \alpha_1 + \alpha_2$. Thus, the local error estimate is defined following (15): $L_{[3]}^{n+1} = \|U_{[4]}^{n+1} - U_{[3]}^{n+1}\|$ and the time step is computed using (16).

Adaptive time step method for the Lawson method

Adaptive methods are more classical in the context of Runge-Kutta methods (see embedded Runge-Kutta methods [22, 21]. In order to perform comparisons with the Hamiltonian splitting, we use methods of same orders as in the splitting context. We will use the Dormand-Prince 4(3) method (DP4(3)) (see [22],[21]) whose Butcher tableau is

0						
$\frac{1}{2}$	$\frac{1}{2}$					
$\frac{1}{2}$	0	$\frac{1}{2}$				
1	0	0	1			
1	$\frac{1}{6}$	$\frac{1}{3}$	$\frac{1}{3}$		$\frac{1}{6}$	
	$\frac{1}{6}$	$\frac{1}{3}$	$\frac{1}{3}$	$\left(\frac{1}{6} - \lambda\right)$	λ	

where λ is a non-zero parameter to be fixed; as in [22] we choose $\lambda = \frac{1}{10}$. The fourth order estimator $U_{[4]}^{n+1}$ is given by the coefficients in the penultimate line (which has to be read as usual in a Butcher tableau) and the third order estimator $U_{[3]}^{n+1}$ is given by the last line. As previously, the local error estimate is defined by $L_{[3]}^{n+1} = \|U_{[4]}^{n+1} - U_{[3]}^{n+1}\|$ as in (15) and the time step is following (16).

4 Vlasov hybrid model: $1dx$-$1dv$ case

In this section, we consider the case of one dimension in space and velocity. Obviously, this simplified framework prevents taking into account several terms of (2)-(5), but it will enable us to study the domain of validity of the VHL system with respect to the original full kinetic model including hot and cold particles. Indeed, even if the velocity mesh induces very costly computations, the $1dx$-$1dv$ case enables to perform them.

First we write down the VHL system in the $1dx - 1dv$ case (see Appendix C for the dimensionless procedure)

$$\begin{cases} \partial_t u_c = E, \\ \partial_t E = -\rho_c^{(0)} u_c - \int_{\mathbb{R}} v f_h \, \mathrm{d}v, \\ \partial_t f_h + v \partial_x f_h + E \partial_v f_h = 0, \end{cases} \tag{17}$$

with the initial conditions (u_c^0, E^0, f_h^0) and $\rho_c^{(0)}$ such that $\partial_x E^0(x) = \rho_c^{(0)} + \int_{\mathbb{R}} f_h^0(x,v)\,\mathrm{d}v - 1$. We introduce the Poisson bracket in this reduced case. For two functionals $\mathcal{F}[u_c, E, f_h]$ and $\mathcal{G}[u_c, E, f_h]$, we get

$$\begin{aligned} \{\mathcal{F}, \mathcal{G}\}[u_c, E, f_h] = & \int_{\mathbb{R}} \int_{\mathbb{R}} f_h \left(\partial_x \frac{\delta \mathcal{F}}{\delta f_h} \partial_v \frac{\delta \mathcal{G}}{\delta f_h} - \partial_v \frac{\delta \mathcal{F}}{\delta f_h} \partial_x \frac{\delta \mathcal{G}}{\delta f_h} \right) \mathrm{d}v\mathrm{d}x \\ & + \int_{\mathbb{R}} \left(\frac{\delta \mathcal{F}}{\delta u_c} \frac{\delta \mathcal{G}}{\delta E} - \frac{\delta \mathcal{F}}{\delta E} \frac{\delta \mathcal{G}}{\delta u_c} \right) \mathrm{d}x \\ & + \int_{\mathbb{R}} \int_{\mathbb{R}} f_h \left(\left(\partial_v \frac{\delta \mathcal{F}}{\delta f_h} \right) \frac{\delta \mathcal{G}}{\delta E} - \left(\partial_v \frac{\delta \mathcal{G}}{\delta f_h} \right) \frac{\delta \mathcal{F}}{\delta E} \right) \mathrm{d}v\mathrm{d}x. \end{aligned}$$

With this framework, the hybrid model (17) can be rewritten as, using $U = (u_c, E, f_h)$,

$$\partial_t U = \{U, \mathcal{H}\}, \quad \text{with } \mathcal{H} = \frac{1}{2} \iint v^2 f_h \, \mathrm{d}v\mathrm{d}x + \frac{1}{2} \int \rho_c^{(0)} u_c^2 \, \mathrm{d}x + \frac{1}{2} \int E^2 \, \mathrm{d}x. \tag{18}$$

4.1 Numerical schemes

In this section, we present two time discretizations of the $1dx$-$1dv$ hybrid model (17). The first one is based on a Hamiltonian splitting whereas the second one belongs to the family of exponential integrators.

4.1.1 Hamiltonian splitting

In this section, we present a numerical method based on a decomposition of the Hamiltonian

$$\mathcal{H} = \underbrace{\frac{1}{2} \iint v^2 f_h \, \mathrm{d}v\mathrm{d}x}_{\mathcal{H}_{f_h}} + \underbrace{\frac{1}{2} \int u_c^2 \, \mathrm{d}x}_{\mathcal{H}_{u_c}} + \underbrace{\frac{1}{2} \int E^2 \, \mathrm{d}x}_{\mathcal{H}_E}.$$

Thus, using $U = (u_c, E, f_h)$, the time *splitting* can be deduced from

$$\partial_t U = \{U, \mathcal{H}_E + \mathcal{H}_{u_c} + \mathcal{H}_{f_h}\} = \{U, \mathcal{H}_E\} + \{U, \mathcal{H}_{u_c}\} + \{U, \mathcal{H}_{f_h}\}, \quad U(t=0) = U_0. \tag{19}$$

In the sequel, we will compute $\varphi^{[E]}$, $\varphi^{[u_c]}$ and $\varphi^{[f_h]}$ the solutions corresponding to each part so that the solution $\varphi(U_0)$ of (19) can be approximated at time t with a first order approximation by the following Lie-Trotter composition

$$U(t) := \varphi_t(U_0) \approx \varphi_t^{[E]} \circ \varphi_t^{[u_c]} \circ \varphi_t^{[f_h]}(U_0). \tag{20}$$

One important remark is that each subsystem can be solved exactly in time such that the error only comes from the splitting which can be reduced by considering high order techniques. Below is detailed the computation of each subflow $\varphi_t^{[E]}(U_0), \varphi_t^{[u_c]}(U_0), \varphi_t^{[f_h]}(U_0)$.

Part $\mathcal{H}_E$

Let us start with $\varphi_t^{[E]}(U_0)$ solution at time t of $\partial_t U = \{U, \mathcal{H}_E\}, U(t=0) = U_0$. We have

$$\begin{aligned} \partial_t u_c &= \{u_c, \mathcal{H}_E\} = E, \\ \partial_t E &= \{E, \mathcal{H}_E\} = 0, \\ \partial_t f_h &= \{f_h, \mathcal{H}_E\} = -E\partial_v f_h. \end{aligned} \tag{21}$$

Starting from an initial solution $U_0 = (u_c, E, f_h)(t=0)$, the solution of this system at time t is

$$\varphi_t^{[E]}(U_0) = \begin{pmatrix} u_c(0) + tE(0) \\ E(0) \\ f_h(0, x, v - tE(0)) \end{pmatrix}.$$

The velocity approximation is performed using a fifth order Lagrange interpolation.

Part $\mathcal{H}_{u_c}$

Next, we consider $\varphi_t^{[u_c]}(U_0)$ the solution at time t of $\partial_t U = \{U, \mathcal{H}_{u_c}\}$. Equations are

$$\begin{aligned} \partial_t u_c &= \{u_c, \mathcal{H}_{u_c}\} = 0, \\ \partial_t E &= \{E, \mathcal{H}_{u_c}\} = -\rho_c^{(0)} u_c, \\ \partial_t f_h &= \{f_h, \mathcal{H}_{u_c}\} = 0. \end{aligned} \tag{22}$$

Starting from an initial solution $U_0 = (u_c, E, f_h)(t=0)$, the solution of this system at time t is

$$\varphi_t^{[u_c]}(U_0) = \begin{pmatrix} u_c(0) \\ E(0) - t\rho_c^{(0)} u_c(0) \\ f_h(0) \end{pmatrix}.$$

Part $\mathcal{H}_{f_h}$

Finally, we write the equations associated with $\partial_t U = \{U, \mathcal{H}_{f_h}\}, U(t=0) = U_0$ (whose solutions at time t is $\varphi_t^{[f_h]}(U_0)$),

$$\begin{aligned} \partial_t u_c &= \{u_c, \mathcal{H}_{f_h}\} = 0, \\ \partial_t E &= \{E, \mathcal{H}_{f_h}\} = -\int_{\mathbb{R}} v f_h \, \mathrm{d}v, \\ \partial_t f_h &= \{f_h, \mathcal{H}_{f_h}\} = -v\partial_x f_h. \end{aligned} \tag{23}$$

Starting from an initial solution $U_0 = (u_c, E, f_h)(t = 0)$, the solution of this system at time t is

$$\varphi_t^{[f_h]}(U_0) = \begin{pmatrix} u_c(0) \\ E(0) - \int_0^t \int_{\mathbb{R}} v f_h(s, x, v)\, \mathrm{d}v \mathrm{d}s \\ f_h(0, x - vt, v) \end{pmatrix}.$$

Regarding the spatial approximation, a spectral method is used. Denoting $\hat{f}_h(t, k, v), k \in \mathbb{Z}$ the Fourier transform of $f_h(t, x, v)$, we approximate $f_h(0, x - vs, v)$ using $\hat{f}_h(s, k, v) = e^{-ikvs}\hat{f}_h(0, k, v)$. Inserting in the equation on E, we get

$$\hat{E}(t, k) = \hat{E}(0, k) - \frac{i}{k} \int_{\mathbb{R}} \left(e^{-ikvt} - 1\right) \hat{f}_h(0, k, v)\, \mathrm{d}v.$$

As mentioned, high order splittings can be constructed from the decomposition (20) (Lie, Strang, Suzuki, ...).

4.1.2 Lawson methods

Here a second time discretization is presented for (17): this is the Lawson method [19]. Indeed, in hyperbolic cases, Lawson methods have to be preferred compared to exponential methods due to stability reasons (see [20]). First we need to reformulate (17), by applying a space Fourier transform on the f_h equation

$$\begin{cases} \partial_t u_c = E \\ \partial_t E = -\rho_c^{(0)} u_c - \int_{\mathbb{R}} v f_h\, \mathrm{d}v \\ \partial_t \hat{f}_h + ikv\hat{f}_h + \widehat{E\partial_v f_h} = 0 \end{cases} \tag{24}$$

where $\hat{f}_h := \hat{f}_h(t, k, v)$ denotes the space Fourier transform of f_h, k being the Fourier variable. Separating the linear and the nonlinear parts, (24) can be rewritten as

$$\partial_t \begin{pmatrix} u_c \\ E \\ \hat{f}_h \end{pmatrix} + \begin{pmatrix} 0 & -1 & 0 \\ \rho_c^{(0)} & 0 & 0 \\ 0 & 0 & ikv \end{pmatrix} \begin{pmatrix} u_c \\ E \\ \hat{f}_h \end{pmatrix} + \begin{pmatrix} 0 \\ \int_{\mathbb{R}} v f_h\, \mathrm{d}v \\ \widehat{E\partial_v f_h} \end{pmatrix} = 0.$$

Let $U = \left(u_c, E, \hat{f}_h\right)^{\mathsf{T}}$ and

$$A = \begin{pmatrix} 0 & -1 & 0 \\ \rho_c^{(0)} & 0 & 0 \\ 0 & 0 & ikv \end{pmatrix}, \qquad N(U) = \begin{pmatrix} 0 \\ \int_{\mathbb{R}} v f_h\, \mathrm{d}v \\ \widehat{E\partial_v f_h} \end{pmatrix}$$

so that (24) can be rewritten in a form amenable to exponential integrators

$$\partial_t U + AU + N(U) = 0.$$

The rest of the algorithm is the same as the one presented in Subsection 3.2. In the numerical results, standard Runge-Kutta methods (like RK(4, 4) or RK(3, 3)) will be used (see also [20]).

Lawson methods are particularly efficient when the linear part can be computed efficiently. This is true in our case since $\exp(tA)$ is explicit

$$e^{tA} = \begin{pmatrix} \cos\left(\sqrt{\rho_c^{(0)}}t\right) & -\frac{\sin\left(\sqrt{\rho_c^{(0)}}t\right)}{\sqrt{\rho_c^{(0)}}} & 0 \\ \sqrt{\rho_c^{(0)}}\sin\left(\sqrt{\rho_c^{(0)}}t\right) & \cos\left(\sqrt{\rho_c^{(0)}}t\right) & 0 \\ 0 & 0 & e^{ikvt} \end{pmatrix}.$$

4.2 Dispersion relation in the hybrid case

This section is devoted to the derivation of the dispersion relation of the hybrid model (17). In the $1dx - 1dv$ case, it is also possible to derive an explicit approximation of the electric field which enables us to validate the code.

We consider an homogeneous stationary state of the hybrid model $(u_c^{(0)}, E^{(0)}, f_h^{(0)}) = (0, 0, f_h^{(0)})$ where $f_h^{(0)}$ only depends on v (see [31], [26]). Then, considering a linearization of the hybrid model around this state $(u_c, E, f_h) = (0, 0, f_h^{(0)}) + \varepsilon(u_c^{(1)}, E^{(1)}, f_h^{(1)})$ and neglecting quadratic terms leads to

$$\begin{cases} \partial_t u_c^{(1)} = E^{(1)}, \\ \partial_t E^{(1)} = -\rho_c^{(0)} u_c^{(1)} - \int v f_h^{(1)} \,\mathrm{d}v, \\ \partial_t f_h^{(1)} + v\partial_x f_h^{(1)} + E^{(1)}\partial_v f_h^{(0)} = 0, \end{cases}$$

with unknown $E^{(1)}$, $u_c^{(1)}$ and $f_h^{(1)}$ which will be denoted E, u_c and f_h respectively, so that the following system will be considered

$$\begin{cases} \partial_t u_c = E, \\ \partial_t E = -\rho_c^{(0)} u_c - \int v f_h \,\mathrm{d}v, \\ \partial_t f_h + v\partial_x f_h + E\partial_v f_h^{(0)} = 0. \end{cases} \tag{25}$$

In the following, we shall consider $\rho_c^{(0)}$ constant and $f_h^{(0)}(v)$ is an even function. The Fourier (resp. Laplace) variable is denoted by k (resp. ω) and the unknown in the Fourier (resp. Laplace) space is denoted with a hat $\hat{\cdot}$ (resp. a tilde $\tilde{\cdot}$). Then, applying Fourier and Laplace transforms to (25) leads to

$$\begin{cases} \tilde{\hat{u}}_c(\omega, k) + \frac{1}{i\omega}\tilde{\hat{E}}(\omega, k) = -\frac{1}{i\omega}\hat{u}_c(t = 0, k), \\ -i\omega\tilde{\hat{E}}(\omega, k) - \hat{E}(t = 0, k) = -\rho_c^{(0)}\tilde{\hat{u}}_c(\omega, k) - \int_{-\infty}^{+\infty} v\tilde{\hat{f}}_h(\omega, k) \,\mathrm{d}v, \\ \tilde{\hat{f}}_h(\omega, k, v) = -\frac{i}{k}\frac{\hat{f}_h(t = 0, k, v)}{v - \frac{\omega}{k}} + \frac{i}{k}\frac{\tilde{\hat{E}}(\omega, k)\partial_v f_h^{(0)}(v)}{v - \frac{\omega}{k}}. \end{cases} \tag{26}$$

Inserting $\tilde{\hat{f}}_h(\omega, k, v)$ into $\int_{-\infty}^{+\infty} v\tilde{\hat{f}}_h(\omega, k)\mathrm{d}v$ requires to pay attention to poles $\omega = kv$, the integral is now considered on a path γ, where γ is either the real axis $(-\infty, +\infty)$ when

$\Im(\omega) > 0$ or an open coutour parallel to the real axis at infinity and passes below the pole ω when $\Im(\omega) \leq 0$. We finally get

$$\tilde{\hat{E}}(\omega, k) = \frac{N(\omega, k)}{D(\omega, k)}$$

where D and N are defined by

$$D(\omega, k) = 1 - \frac{1}{k^2}\left(\rho_c^{(0)}\frac{k^2}{\omega^2} + \int_\gamma \frac{\partial_v f_h^{(0)}(v)}{v - \frac{\omega}{k}}\,\mathrm{d}v\right) \tag{27}$$

and

$$N(\omega, k) = \frac{\rho_c^{(0)}}{\omega^2}\hat{u}_c(t=0,k) - \frac{1}{i\omega}\hat{E}(t=0,k) - \frac{1}{\omega k}\int_\gamma v\frac{\hat{f}_h(t=0,k,v)}{v - \frac{\omega}{k}}\,\mathrm{d}v. \tag{28}$$

For a given k, the roots $\omega \in \mathbb{C}$ of $D(k, \omega)$ enables to get the time behavior of the kth Fourier mode of the electric field.

Consistency between full kinetic and VHL models

This approach enables us to validate the VHL model (17) with respect to the full kinetic model when $T_c \to 0$. Indeed, starting from the full Vlasov-Poisson system

$$\begin{cases} \partial_t f + v\partial_x f + E\partial_v f = 0, \\ \partial_x E = \int_{\mathbb{R}} f\,\mathrm{d}v - 1, \end{cases} \tag{29}$$

a similar linearization procedure gives $\tilde{\hat{E}}^{VP}(\omega, k) = \frac{N^{VP}(k,\omega)}{D^{VP}(k,\omega)}$ with

$$D^{VP}(\omega, k) = 1 - \frac{1}{k^2}\int_\gamma \frac{\partial_v f^0(v)}{v - \frac{\omega}{k}}\,\mathrm{d}v, \quad N^{VP}(\omega, k) = -\frac{1}{k^2}\int_\gamma \frac{\hat{f}(t=0,k,v)}{v - \frac{\omega}{k}}\,\mathrm{d}v. \tag{30}$$

Now, if initial conditions are compatible, we have the following proposition.

Proposition 1. *If $f^0(v) = f_h^0(v) + f_c^0(v)$ with*

$$f_c^0(v) = \rho_c^{(0)}\delta_{v=0}(v) = \lim_{T_c \to 0} \frac{\rho_c^{(0)}}{(2\pi T_c)^{1/2}} \exp\left(-\frac{|v|^2}{2T_c}\right),$$

then $D^{VP}(\omega, k) = D(\omega, k)$. In particular, they have same roots.

Proof. Since $D^{VP}(\omega, k) = 1 - \frac{1}{k^2}\left(\int_\gamma \frac{\partial_v f_c^0(v)}{v - \frac{\omega}{k}}\,\mathrm{d}v + \int_\gamma \frac{\partial_v f_h^0(v)}{v - \frac{\omega}{k}}dv\right)$, we have to prove that $\int_\gamma \frac{\partial_v f_c^0(v)}{v - \frac{\omega}{k}}\,\mathrm{d}v = \rho_c^{(0)}\frac{k^2}{\omega^2}$. Let us denote $\mathcal{M}_{\rho,u,T}(v) := \frac{\rho}{(2\pi T)^{\frac{1}{2}}}\exp\left(-\frac{|v-u|^2}{2T}\right)$. Then $\partial_v \mathcal{M}_{\rho_c^{(0)},0,T_c}(v) = -\frac{v}{T_c}\mathcal{M}_{\rho_c^{(0)},0,T_c}(v)$ and

$$\int_\gamma \frac{\partial_v \mathcal{M}_{\rho_c^{(0)},0,T_c}(v)}{v - \frac{\omega}{k}}\,\mathrm{d}v = -\frac{\rho_c^{(0)}}{T_c}\left(1 + \frac{1}{\sqrt{2T_c}}\frac{\omega}{k}Z\left(\frac{1}{\sqrt{2T_c}}\frac{\omega}{k}\right)\right),$$

where Z is the plasma dispersion function defined by $Z(\xi) = \frac{1}{\sqrt{\pi}} \int_\gamma \frac{e^{-z^2}}{z-\xi} \, \mathrm{d}z = \sqrt{\pi} \exp(-\xi^2)(i - \mathrm{erfi}(\xi))$. When $\xi \to +\infty$, we have $\mathrm{erfi}(\xi) = -i + \exp(\xi^2)/\sqrt{\pi}(\frac{1}{\xi} + \frac{1}{2\xi^3} + \frac{3}{4\xi^5} + \mathcal{O}(\xi^{-7}))$, so that $\xi Z(\xi)$ is equivalent to $-1 - \frac{1}{2\xi^2} + \mathcal{O}(\xi^{-4})$. With $\xi = \frac{1}{\sqrt{2T_c}} \frac{\omega}{k}$, we obtain

$$\lim_{T_c \to 0} \int_\gamma \frac{\partial_v \mathcal{M}_{\rho_c^{(0)},0,T_c}(v)}{v - \frac{\omega}{k}} \, \mathrm{d}v = \rho_c^{(0)} \frac{k^2}{\omega^2}.$$

When considering the Dirac expression, an integration by parts formula gives

$$\int_\gamma \frac{\partial_v(\rho_c^{(0)} \delta_{v=0}(v))}{v - \frac{\omega}{k}} \, \mathrm{d}v = \rho_c^{(0)} \int_\gamma \delta_{v=0}(v) \frac{1}{\left(v - \frac{\omega}{k}\right)^2} \, \mathrm{d}v = \rho_c^{(0)} \frac{k^2}{\omega^2}.$$

From both point of view (cold limit or Dirac mass), we get the result. □

Explicit expression of the linearized electric field

We can go further by deriving an explicit approximation of the electric field. This is the goal of the end of this part. Appealing the residue theorem, we can compute the inverse Laplace transform

$$\hat{E}(t,k) = \frac{1}{2i\pi} \int_{u-i\infty}^{u+i\infty} \tilde{\hat{E}}(\omega,k) e^{-i\omega t} \, \mathrm{d}\omega = \sum_j Res_{\omega=\omega^{k,j}} \left(\tilde{\hat{E}}(\omega,k) e^{-i\omega t} \right)$$

where u is a real number so that the contour path of integration is in the region of convergence of $\tilde{\hat{E}}(\omega,k)$ and where $\omega^{k,j}$ are the poles of $\tilde{\hat{E}}(\omega,k)$ (or the roots of $D(k,\omega)$). If $\omega^{k,j}$ is a simple pole, we have

$$\begin{aligned} Res_{w=w^{k,j}} \left(\tilde{\hat{E}}(\omega,k) e^{-i\omega^{k,j} t} \right) &= \lim_{\omega \to \omega^{k,j}} \left(\omega - \omega^{k,j} \right) \tilde{\hat{E}}(\omega,k) e^{-i\omega t} \\ &= \lim_{\omega \to \omega^{k,j}} \left(\omega - \omega^{k,j} \right) \frac{N(k,\omega)}{D(k,\omega)} e^{-i\omega t}. \end{aligned}$$

Thus, using a Taylor expansion of $D(k,\omega)$ around $w^{k,j}$ gives

$$D(k,\omega) = \underbrace{D(k,\omega^{k,j})}_{0} + \left(\omega - \omega^{k,j} \right) \frac{\partial D}{\partial \omega}(k,\omega^{k,j}) + \mathcal{O}\left((\omega - \omega^{k,j})^2 \right)$$

and finally

$$Res_{\omega=\omega^{k,j}} \left(\tilde{\hat{E}}(\omega,k) e^{-i\omega^{k,j} t} \right) = \frac{N(k,\omega^{k,j})}{\frac{\partial D}{\partial \omega}(k,\omega^{k,j})} e^{-i\omega^{k,j} t}. \tag{31}$$

Remark 1. *In practice, for a given wavenumber k, we obtain a very good approximation of $\hat{E}(t,k)$ considering only the dominant frequency (with the largest imaginary part). Indeed, denoting $\omega_\pm^{k,j_0} = \pm\omega_r + i\omega_i$ this dominant frequency, for any other frequency $\omega^{k,j}$ such that $\Im(\omega^{k,j}) < \omega_i$, we get (using the notation $C_j = N(k,\omega^{k,j})/\frac{\partial D}{\partial \omega}(k,\omega^{k,j})$)*

$$\begin{aligned} \hat{E}(t,k) = & \sum_j C_j e^{-i\omega^{k,j} t} = C_{j_0^+} e^{-i\omega_+^{k,j_0} t} + C_{j_0^-} e^{-i\omega_-^{k,j_0} t} + \sum_{j \neq j_0^\pm} C_j e^{-i\omega^{k,j} t} \\ = & \; e^{\omega_i t} \left(C_{j_0^+} e^{-i\omega_r t} + C_{j_0^-} e^{i\omega_r t} + \sum_{j \neq j_0^\pm} C_j e^{-i\Re(\omega^{k,j}) t} e^{(\Im(\omega^{k,j}) - \omega_i) t} \right) \end{aligned}$$

and since $\Im(\omega^{k,j}) - \omega_i < 0 \ \forall j \neq j_0^{\pm}$*, we deduce the sum goes to zero for large times.*

Thanks to this remark, we only consider the root with the largest imaginary part, and under the assumption $f_h^{(0)}$ is even, one can prove that if $\omega = \omega_r + i\omega_i$ is a (simple) root, then the same is true for $-\omega_r + i\omega_i$. We deduce the following approximation of the Fourier transform of the electric field

$$\hat{E}(t,k) \approx Res_{\omega=\omega_r+i\omega_i}\left(\tilde{\hat{E}}(\omega,k)e^{-i\omega t}\right) + Res_{\omega=-\omega_r+i\omega_i}\left(\tilde{\hat{E}}(\omega,k)e^{-i\omega t}\right)$$

where the residues are defined by (31). Let denote $r^{\pm}$ the modulus of $\frac{N(k,\pm\omega_r+i\omega_i)}{\frac{\partial D}{\partial\omega}(k,\pm\omega_r+i\omega_i)}$ and $\phi^{\pm}$ its argument, we then get

$$\hat{E}(t,k) \approx r^+ e^{i\phi^+} e^{-i(\omega_r+i\omega_i)t} + r^- e^{i\phi^-} e^{-i(-\omega_r+i\omega_i)t}. \tag{32}$$

In the tests we will consider, the perturbation is a trigonometric function which enables to compare easily (32) with the numerical results.

4.3 Numerical results

This section is devoted to the study of numerical methods presented in Subsection 4.1 for the $1dx$-$1dv$ hybrid model (17). First of all, the validity of hybrid model is discussed. Then, splitting and Lawson methods are compared, in both constant and adaptive time step cases. In the following, we denote by $\alpha \in [0,1]$ the density of hot particles and by $1-\alpha = \rho_c^{(0)}$ the density of cold particles.

Using the following notation for the Maxwellian

$$\mathcal{M}_{\rho,u,T}(v) := \frac{\rho}{(2\pi T)^{\frac{1}{2}}} \exp\left(-\frac{|v-u|^2}{2T}\right),$$

we will consider in this section the following initial condition for the full kinetic model

$$f(t=0,x,v) = \mathcal{M}_{1-\alpha,0,T_c}(v) + (1+\epsilon\cos(kx))\left(\mathcal{M}_{\alpha/2,v_0,1}(v) + \mathcal{M}_{\alpha/2,-v_0,1}(v)\right) \tag{33}$$

with $k = 0.5$, $v_0 = 3.4$, $\alpha = 0.2$, $x \in [0,L]$, $L = 2\pi/k = 4\pi$, $v \in [-v_{\max}, v_{\max}]$ ($v_{\max} = 12$) and the perturbation for the hot particles is $\epsilon = 10^{-2}$. The parameter T_c will vary to study the limit as T_c goes to zero. For the hybrid model, the compatible initial condition reads

$$\begin{aligned} u_c(t=0,x) &= 0 \\ f_h(t=0,x,v) &= (1+\epsilon\cos(kx))\left(\mathcal{M}_{\alpha/2,v_0,1}(v) + \mathcal{M}_{\alpha/2,-v_0,1}(v)\right) \end{aligned} \tag{34}$$

where k, v_0, α and ϵ are chosen as in the full kinetic case. We easily check that, taking the limit $T_c \to 0$ in (33) gives $f(t=0,x,v) = f_c(t=0,x,v) + f_h(t=0,x,v)$, with $f_h(t=0,x,v)$ given by (34) and $f_c(t=0,x,v) = (1-\alpha)\delta_{v=0}$. The initial electric field $E(t=0,x)$ is obtained by solving the Poisson equation at initial time

$$\partial_x E(t=0) = (1-\alpha) + \int (1+\epsilon\cos(kx))\left(\mathcal{M}_{\alpha/2,v_0,1}(v) + \mathcal{M}_{\alpha/2,-v_0,1}(v)\right) \mathrm{d}v - 1. \tag{35}$$

We will denote N_x (resp. N_v) the number of points in the space (resp. velocity) variable such that the space mesh is $\Delta x = L/N_x$ (resp. the velocity mesh is $\Delta v = 2v_{\max}/N_v$).

4.3.1 Numerical study of the limit of the full kinetic model towards the hybrid model

Our goal is to investigate numerically the convergence of the full kinetic model (29) towards the hybrid model as the temperature of the cold particles T_c goes to zero.

A first consistency study has been done on dispersion relations (see Proposition 1). Here, we propose another validation at the numerical level on the full nonlinear models. On Figure 1, we plot the time evolution of the electric energy $\|E(t,\cdot)\|_{L^2} = \frac{1}{2}\int_0^L E^2(t,x)\,\mathrm{d}x$ in semi-log scale. The numerical parameters are chosen as follows: $N_x = 135$, $N_v = 1011$, $\Delta t = 0.05$. A large number of points is considered in the velocity direction to correctly describe the Maxwellian with different temperatures $T_c = 0.05, 0.1, 0.2, 0.4$. For the two models (full kinetic and hybrid), a Lawson RK(4, 4) time integrator is used, with a spectral approximation in space and a WENO approximation in velocity.

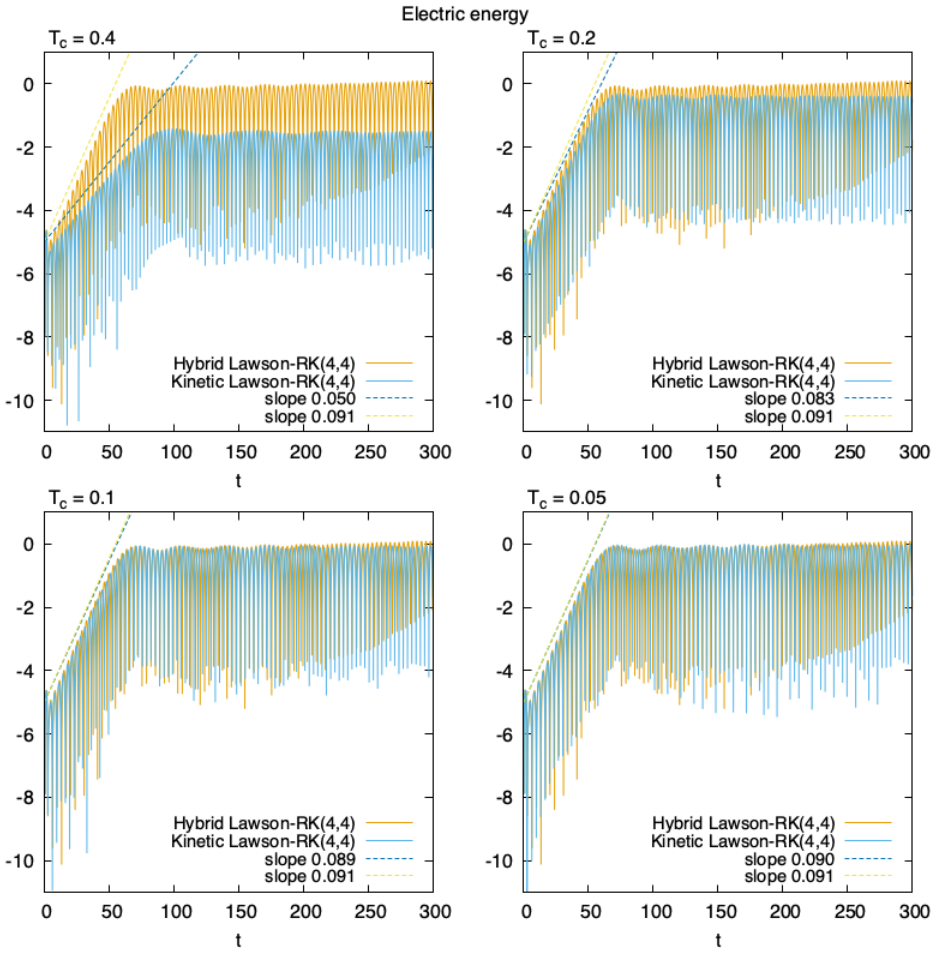

Figure 1: Time evolution of the electric energy for the full kinetic model (with different values of $T_c = 0.4, 0.2, 0.1, 0.05$) and the hybrid model.

First we observe a very good agreement between the two models when the cold temperature T_c is small enough ($T_c = 0.05, 0.1$), which validates the hybrid modeling. The

perturbation of the hot particles generates an instability (two-stream type instability) which is developing up to $t = 60$ and a nonlinear phase takes place up to $t = 300$. The instability rate of the linear phase can be computed a priori by solving the dispersion relation. The dominant frequency is computed by solving the dispersion relation using a Newton method and written in Table 1. The corresponding slopes are plotted on Figure 1: Lawson schemes are able to recover very accurately the instability rates computed from the linear theory. One can also remark that, when T_c is lower than 0.1, the results obtained from the full kinetic model and the hybrid model are very close to each other, even in the nonlinear phase.

We can go further with the dispersion relation by reconstructing the linearized electric field E_{lin} from (32). We have $E_{\text{lin}}(t,x) = 4\epsilon r^+ e^{\omega_i t}\cos(\omega_r t - \phi^+)\cos(kx)$. We are then able to compare electric energy obtained by Lawson method to the fully linearized electric energy given by dispersion relation and equal to $4\sqrt{2\pi}\epsilon r^+ e^{\omega_i t}|\cos(\omega_r t - \phi^+)|$ (with $r^+ = 0.0461822286329758, \phi^+ = 1.08935392582393, \omega_r = 0.9054349300445959, \omega_i = 0.0909886498164638$ computed numerically from the dispersion relation). Results are presented on Figure 2; parameters are the same as previously, except the perturbation $\epsilon = 10^{-5}$ which is smaller to increase the linear phase. One can observe a very good agreement between numerical and analytical results up to time $t \approx 120$ which corresponds to the beginning of the nonlinear phase (which can not be reproduced by the linear theory).

T_c	$\omega(T_c)$
0.4	$1.06 + i0.05$
0.2	$0.98 + i0.083$
0.1	$0.94 + i0.089$
0.05	$0.92 + i0.09$
hybrid ($T_c = 0$)	$0.90 + i0.091$

Table 1: Solution of dispersion relation for different values of T_c in kinetic case (30), and for hybrid case (27).

On Figure 3, we plot the distribution function obtained by the kinetic (with $T_c = 0.05$) and hybrid models at time $t = 0$ and $t = 300$. For the hybrid model, we plot both f_h and u_c whereas for the kinetic model, we only plot the values of f which are lower than 0.2. We can see a very good agreement on both the distribution function (the two vortices are created around the phase velocity $v_\phi \approx Re(\omega)/k = 1.84$) and on the cold velocity. Whereas the capability of the hybrid model to capture the linear phase of the full kinetic model can be deduced from the dispersion relation, its capability to capture correctly the nonlinear effects is more delicate to anticipate. Figure 3 illustrates well the efficiency of the hybrid modelling.

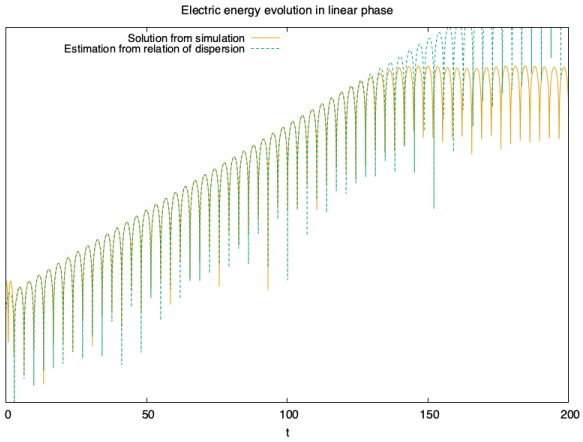

Figure 2: Comparison of electric energy given by Lawson method on hybrid model, and by reconstruction of linearized electric field from dispersion relation study.

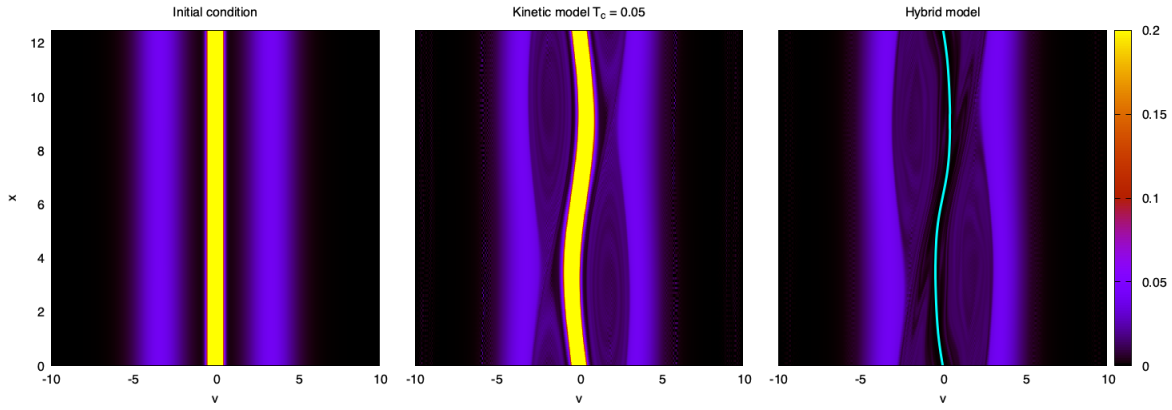

Figure 3: Density particles f in phase space at initial time (left), at final time $t = 300$ computed by kinetic model (middle), and density of hot particles f_h at $t = 300$ computed by hybrid model (right) (in cyan is plotted the mean velocity of cold particles u_c).

4.3.2 Comparison of the two solvers

This section is devoted to the comparison of the Hamiltonian splitting method presented in Subsection 4.1.1 and the Lawson method presented in Subsection 4.1.2 for the numerical resolution of linearized hybrid model (17).

We consider initial condition (34) with $k = 0.5$, $\alpha = 0.2$, $v_0 = 3.4$, $x \in [0, L], L = 4\pi$, $v \in [-12, 12]$ and the perturbation $\epsilon = 10^{-2}$. The initial electric field $E(t = 0, x)$ is obtained by solving Poisson equation (35) at $t = 0$. In the following, phase-space domain is discretized with $N_x = 27$ points in x and $N_v = 128$ points in v.

Concerning the time step, we consider three time steps:

- $\Delta t = 0.1 \approx 0.5\Delta v$; this is a CFL condition from standard finite volume schemes.
- $\Delta t = 0.5 \approx \sigma \frac{\Delta v}{\|E^n\|_\infty} = 0.54$, with $\sigma \approx 1.732$; this is the CFL condition of WENO5 with RK(4,4) (see [20]) computed from the numerical estimate $\|E^n\|_\infty = \max_{i,n} |E_i^n| \approx 0.6$.
- $\Delta t = 0.7$; this is a large time step chosen to illustrate that the splitting methods have no stability constraint on the time step.

On Figure 4, we can see the time evolution of the electric energy (in semi-log scale) obtained by the two fourth order (Suzuki (11)-(12) and Lawson-RK(4, 4)) solvers with the time steps $0.1, 0.5$ and 0.7. First, it is important to note that all the simulations capture correctly the linear phase, even with a coarse mesh and large time steps. Moreover, for $\Delta t = 0.1, 0.5$, both methods are stable as expected and give very similar results. However, for $\Delta t = 0.7$ Lawson-RK(4,4) method becomes unstable in the nonlinear phase; indeed, in this regime, the electric field amplitude reaches the maximum and $\Delta t = 0.7$ violates the CFL condition, whereas Suzuki splitting method stays stable as expected.

On Figure 5 we plot the time evolution of the relative error on total energy, computed as

$$\frac{\mathcal{H}^n}{\mathcal{H}^0} - 1 \tag{36}$$

with

$$\mathcal{H}^n = \frac{1}{2} \iint v^2 f_h^n \, \mathrm{d}v\mathrm{d}x + \frac{1}{2} \int \rho_c^{(0)} (u_c^n)^2 \, \mathrm{d}x + \frac{1}{2} \int (E^n)^2 \, \mathrm{d}x.$$

We consider the same numerical parameters as before and compare the effect of the time integrators (Hamiltonian splittings: Lie (9), Strang (10) and Suzuki (11), and Lawson-RK(4, 4)) on the total energy preservation. Firstly, we can observe on Figure 5 that the energy is very well preserved by splitting methods; in particular, the relative error oscillates around a constant for large times, which is a typical behavior of geometric methods. Secondly, for time steps under CFL condition, the error obtained when using Lawson-RK(4,4) method is near 4% which is very acceptable. Obviously, as noticed previously, when $\Delta t = 0.7$ we can observe that error on Lawson-RK(4,4) diverges in the nonlinear phase due to the numerical instability but before that, the error is about 2%. Finally, in Table 2, the maximum of the relative error $\max_n |\mathcal{H}^n/\mathcal{H}^0 - 1|$ for the different methods and time steps is shown.

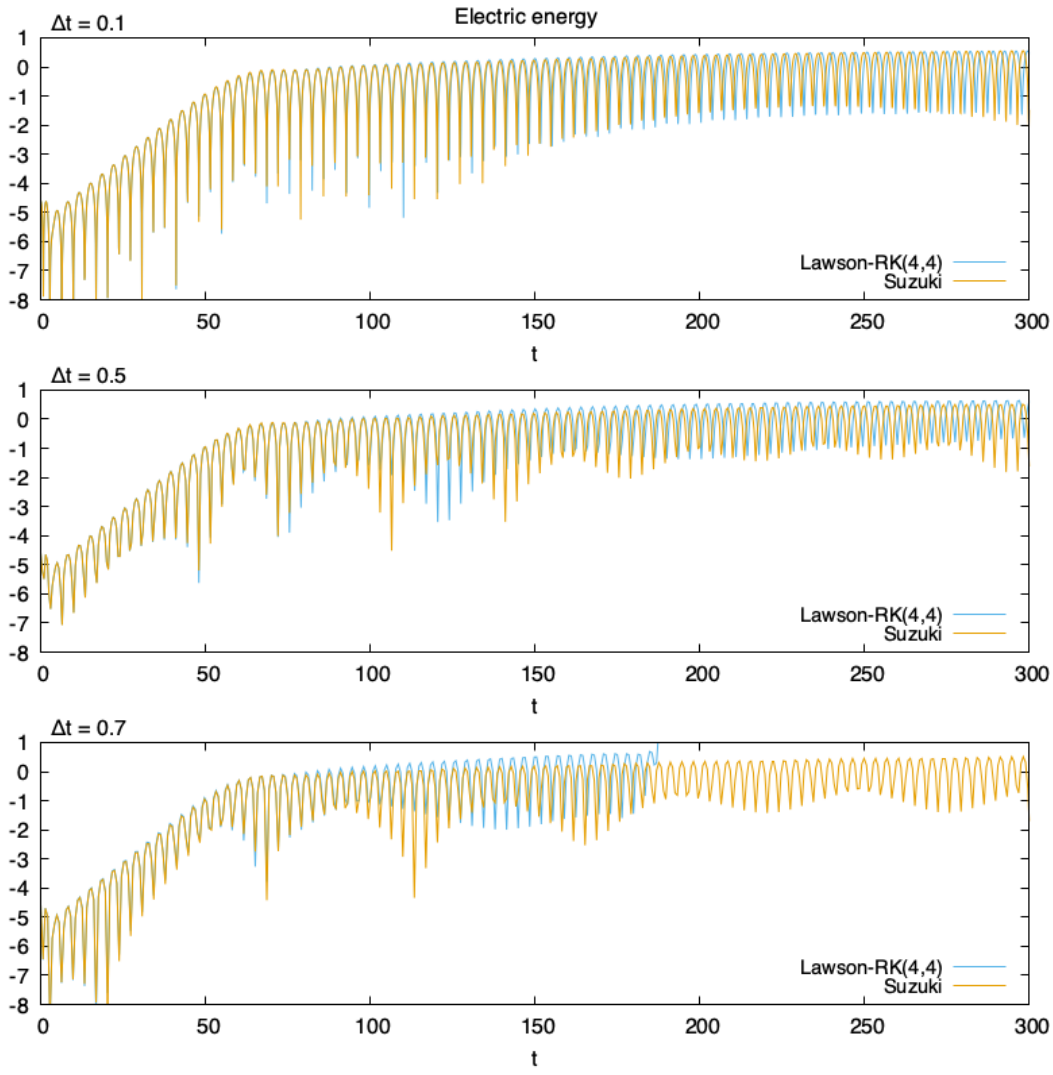

Figure 4: Time evolution of the electric energy for the hybrid model (computed by the Lawson and Suzuki methods) for different choices of time step $\Delta t = 0.1, 0.5, 0.7$).

We compare in Figure 6 the distribution of hot particles f_h computed by Suzuki and Lawson-RK(4,4) method at time $t = 100$, on which we added the mean velocity of cold particles u_c (we have chosen $\Delta t = 0.1$). A very good agreement of the two numerical solutions is observed: the vortices position and the cold velocity shape are very close for both methods. We can also observe that the Lawson-RK(4,4) method seems to introduce slightly more diffusion than Suzuki since the vortices have a better resolution. This might be explained by the velocity discretization of the two methods; in the Lawson-RK(4, 4) method, a WENO5 method (involving slope limiters) is used whereas a 5-th order reconstruction (without limiters) is used in Suzuki method.

To complete this part, we plot in Figure 7 the orders of accuracy of different time integrators used to approximate the hybrid model: Hamiltonian splittings (Lie, Strang and Suzuki) and Lawson (RK(4, 4) and RK(3, 3)). To do so, we computed the maximum value of relative error on total energy $\max_n |\mathcal{H}^n/\mathcal{H}^0 - 1|$, until time $t = 15$ as a function

	0.1	0.5	0.7
Lie	0.0036	0.0187	0.0394
Strang	0.0001	0.0019	0.0109
Suzuki	3×10^{-8}	0.0001	0.0028
Lawson-RK(4,4)	0.0372	0.0331	`NaN`

Table 2: Maximum of relative error for different simulations of Figure 5.

of different time steps chosen in the interval $\Delta t \in [0.01, 1.25]$ (here we have $N_x = 243$ and $N_v = 512$). All the theoretical orders are recovered and we also observe that the error constants of Suzuki and Lawson-RK(4,4) methods are very close. Let us remark that the Suzuki method is a bit more expensive than the Lawson-RK(4,4) method (more details will be given in Subsection 4.3.4).

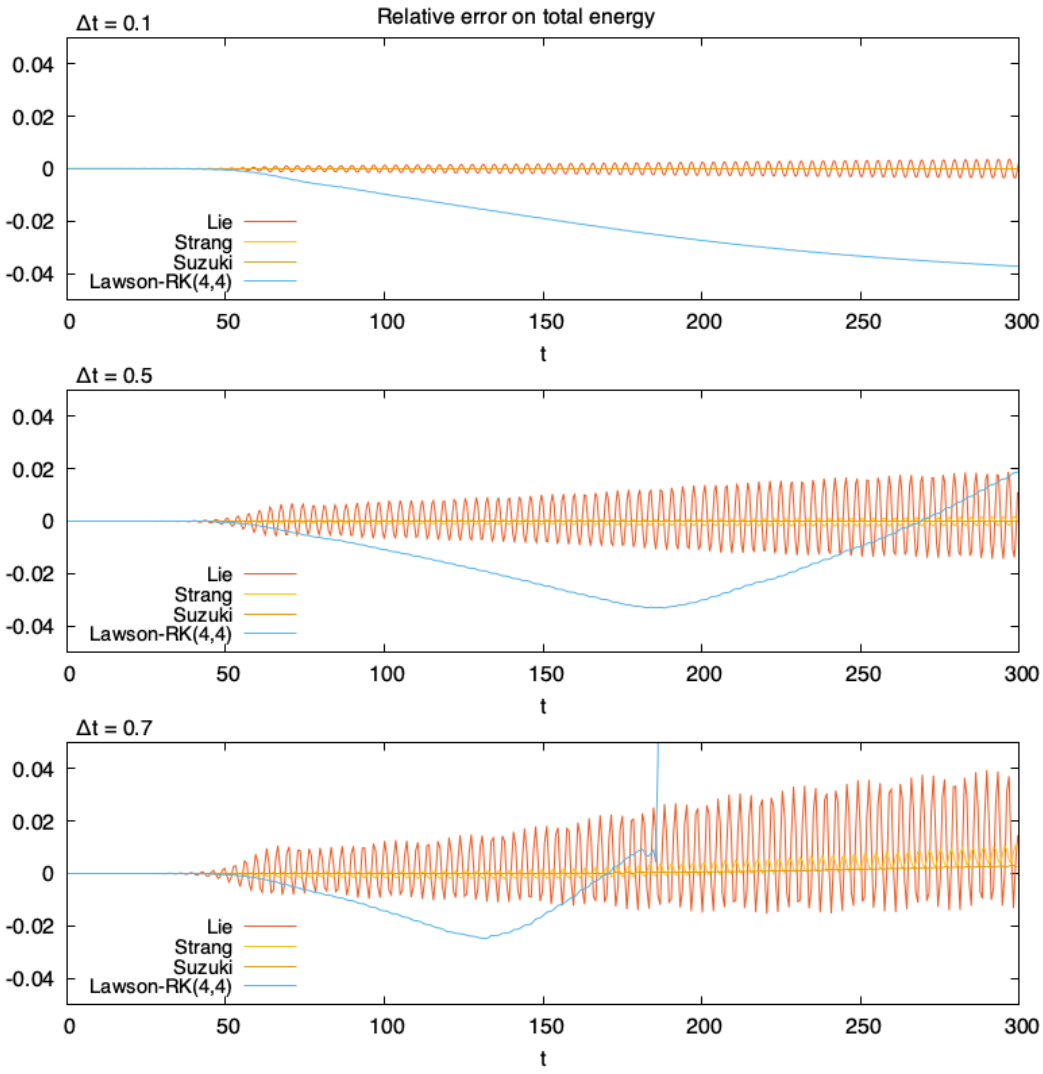

Figure 5: Time evolution of the relative error on total energy for the hybrid model (computed by Lawson and splitting methods and for different choices of time step $\Delta t = 0.1, 0.5, 0.7$).

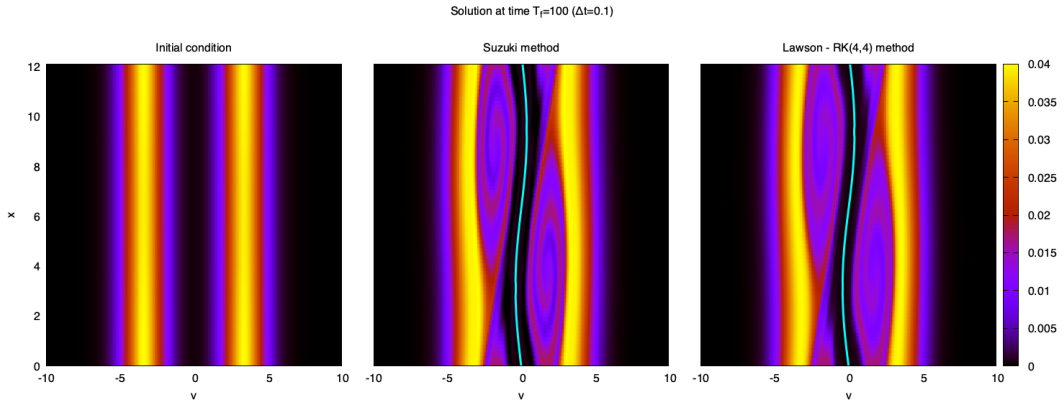

Figure 6: Density of hot particules f_h and mean velocity of cold particules u_c (cyan curves) at initial time (left), at time $t = 100$ computed by Suzuki method (middle) and computed by Lawson-RK(4,4) method (right).

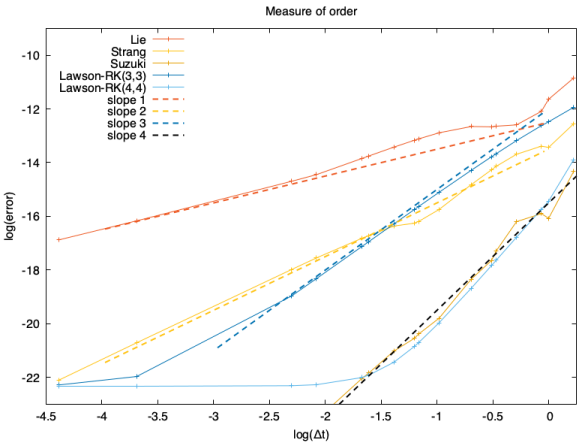

Figure 7: Study of order in time of different numerical methods for the hybrid model (Lawson and splitting methods). The error is computed on maximum value of relative error on total energy.

4.3.3 Comparison of the two adaptive time step methods

This section is devoted to the study of the Suzuki and Lawson methods combined with adaptive time step strategies. Both methods are presented in Subsection 3.3. For all simulations, we are interested in error estimator (15) which we recall in our hybrid model case

$$L_{[3]}^{n+1} = \left(\sum_{i=0}^{N_x-1} ({u_c}_i^{n+1,[4]} - {u_c}_i^{n+1,[3]})^2 \Delta x \right)^{\frac{1}{2}} + \left(\sum_{i=0}^{N_x-1} (E_i^{n+1,[4]} - E_i^{n+1,[3]})^2 \Delta x \right)^{\frac{1}{2}} + \left(\sum_{i=0}^{N_x-1} \sum_{j=0}^{N_v-1} \left| {f_h}_{i,j}^{n+1,[4]} - {f_h}_{i,j}^{n+1,[3]} \right|^2 \Delta v \Delta x \right)^{\frac{1}{2}} = L_{u_c}^{n+1} + L_E^{n+1} + L_{f_h}^{n+1}, \tag{37}$$

where ${u_c}_i^{n+1,[p]}$, $E_i^{n+1,[p]}$ and ${f_h}_{i,j}^{n+1,[p]}$ are the discrete unknown computed with a p-order method in time and associated to time t^{n+1} and to the phase space grid point $x_i = i\Delta x, i = 0, \ldots, N_x$ and $v_j = -v_{\max} + j\Delta v, j = 0, \ldots, N_v$. For both methods, at iteration n, if the error criteria $\|L_{[3]}^{n+1}\| <$tol is fullfiled, then the time step Δt_{n+1} at the next iteration is computed using (16). This will allow us to compare the error estimate with the same tolerance tol (we considered a tolerance equal to tol$= 2 \times 10^{-5}$) for the DP4(3) method and the Suzuki method. We will also look at the number of iterations of each simulation method, and the size of the time steps that the adaptive time step method proposes. Note that the two methods in Section 3.3 use the same error estimation so that they share the criterion for rejecting an iteration.

method	number of iterations	number of succeeded iterations	ratio
Suzuki	23895	23849	0.998
Lawson-DP4(3)	2288	2192	0.958

Table 3: Comparison of number of iterations to solve the problem to time $t = 300$, succeeded iterations of adaptive time step methods and ratio between succeeded and total numbers of iterations.

On Table 3, we show the number of iterations needed to reach the final time $t = 300$ for the two adaptive time step methods (Suzuki and Lawson-DP4(3)) using the following numerical parameters $N_x = 81, N_v = 128$. We also give the number of rejected iterations and the ratio of succeeded iterations of adaptive time step method over the total number of iterations. First, we observe that a large majority of iterations are accepted for both methods, which means that the error estimate is efficient. For Lawson-DP4(3), the ratio is slightly lower than for Suzuki, which means that the strategy tries larger time steps which are sometimes rejected. The very high proportion of accepted iterations implies that we rarely have to modify time step and compute again the same iteration with a smaller time step. The corresponding overcost is neglectable. The second remark is that the Suzuki method needs about 10 times more iterations than Lawson-DP4(3) method, meaning that Suzuki requires smaller time steps to satisfy the criterion $\|L_{[3]}^{n+1}\| <$tol.

On Figure 8, the time history of the time steps is represented (rejected iterations are also presented using square boxes) for both adaptive methods. First, we observe

that larger time steps are computed during the linear phase (up to $t \approx 50$). During the nonlinear phase, the time step becomes smaller and oscillates around a constant, which enables to capture nonlinear effects and strong gradients. Second, for a same tolerance (tol=2×10^{-5}), we can see that Suzuki needs smaller time steps compared to DP4(3) to guarantee that the criterion is satisfied, as remarked previously in Table 3. Note that the variations of the time step are quite important; it is possible to control these variations by incorporating bounds in the predicted time steps, which in addition enables to reduce the number of rejected iterations (see [23]). On Figure 9, we plot the local error $L_{[3]}$ as a function of time for Lawson methods (left) and Suzuki methods (right), with adaptive and constant time steps. For a large time step ($\Delta t = 0.5$), even if the methods are stable, the local error is larger than the tolerance (still equal to 2×10^{-5}) whereas the adaptive methods automatically choose the optimal step for which the local error is smaller than the tolerance, as expected. One can see that the Lawson method with adaptive stepping strategy and with a fixed time step $\Delta t = 0.1$ leads to very close results; however, the adaptive version optimizes the size of the time step according to the local error which is a nice feature in this case. For Suzuki methods, as already discussed, smaller time steps are required to respect the tolerance compared to DP4(3). Moreover, with $\Delta t = 0.1$ constant, Suzuki creates larger local error whereas DP4(3) remains (almost) under the tolerance.

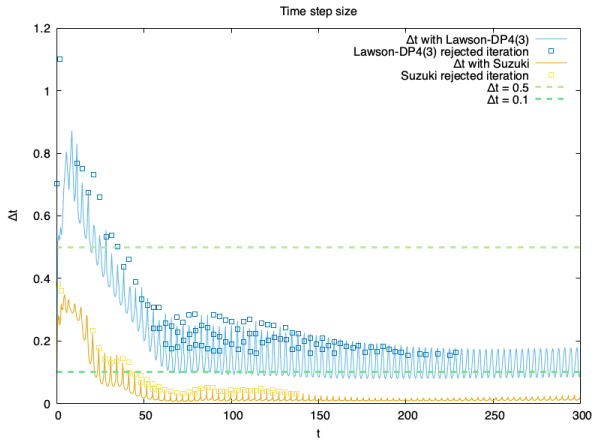

Figure 8: Time evolution of the time step size Δt_n (rejected iterations are denoted by squares) for the hybrid model with adaptive time stepping methods.

For the two adaptive methods, we are now interested in the evolution of the local error over time, but looking at the different contributions of the local error $L^n_{[3]}$, namely $L^n_{u_c}$, L^n_E and $L^n_{f_h}$ in (37). The results are shown in Figure 10. The error of DP4(3) and its various contributions are shown at the top, while these of the Suzuki method are shown at the bottom. One observes that the contribution from $L^n_{u_c}$ is negligible which can be explained by the fact that in DP4(3), the linear part of the problem is solved exactly. However, since the nonlinear part includes the calculation of the current $\int v f_h \, \mathrm{d}v$ in L^n_E and the transport in the v direction in $L^n_{f_h}$, the contribution of these two components remains preponderant throughout the simulation. For Suzuki method, the error comes essentially from $L^n_{f_h}$ because of the error from the transport part interpolation.

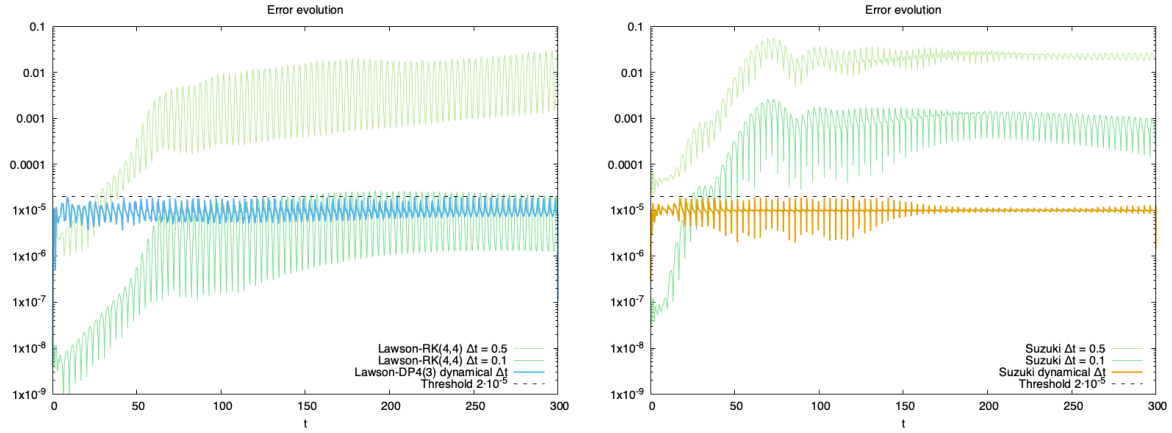

Figure 9: Comparison of time error evolution for constant and adaptive time step approaches. Lawson methods on the left, Suzuki methods on the right (semi-log scale).

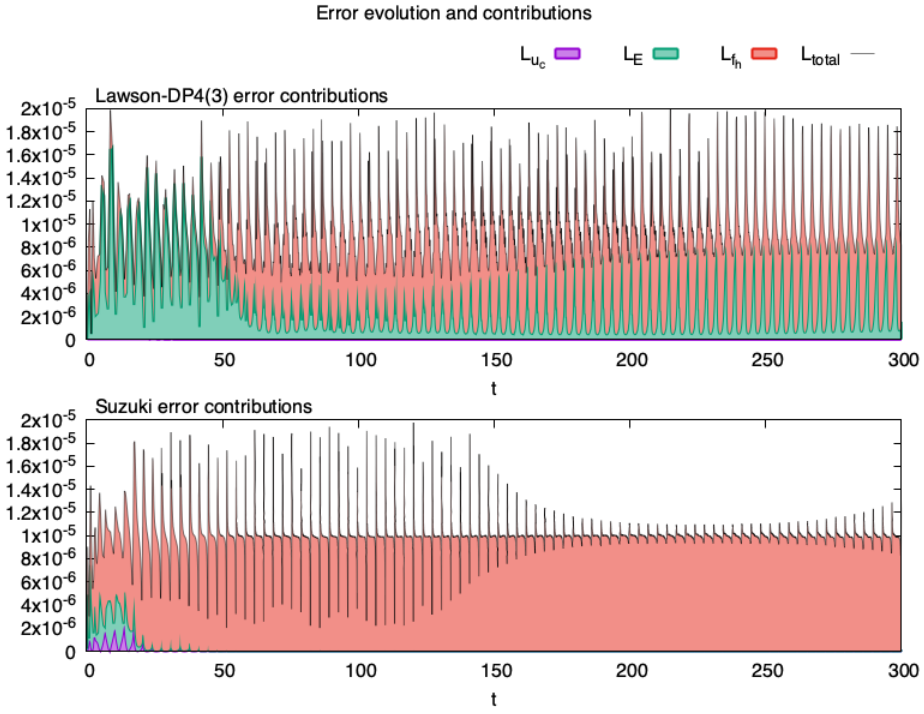

Figure 10: Comparison of each component of local error as a function of time for Lawson (top) and Suzuki (bottom).

4.3.4 About computational time

To end the comparison between splitting and Lawson methods, we focus on their computational times. On Figure 11 (left), we present the mean value as well as quartiles of the computational time of one iteration for the RK(4, 4), DP4(3) and Suzuki methods. We recall that RK(4,4) method is constituted of four stages, whereas DP4(3) and Suzuki methods have 5 stages. This explains why one iteration of RK(4,4) method costs less than one iteration of two other methods. On the right part of Figure 11, we look at each stage of the methods. We recall that DP4(3) is made of 4 steps of RK(4,4) plus a fifth extra step. As expected, all steps of Suzuki method have the same cost (since Suzuki is a composition of 5 Strang splittings). On the contrary, we observe that the first two steps of RK(4,4) or DP4(3) are less costly than last steps.

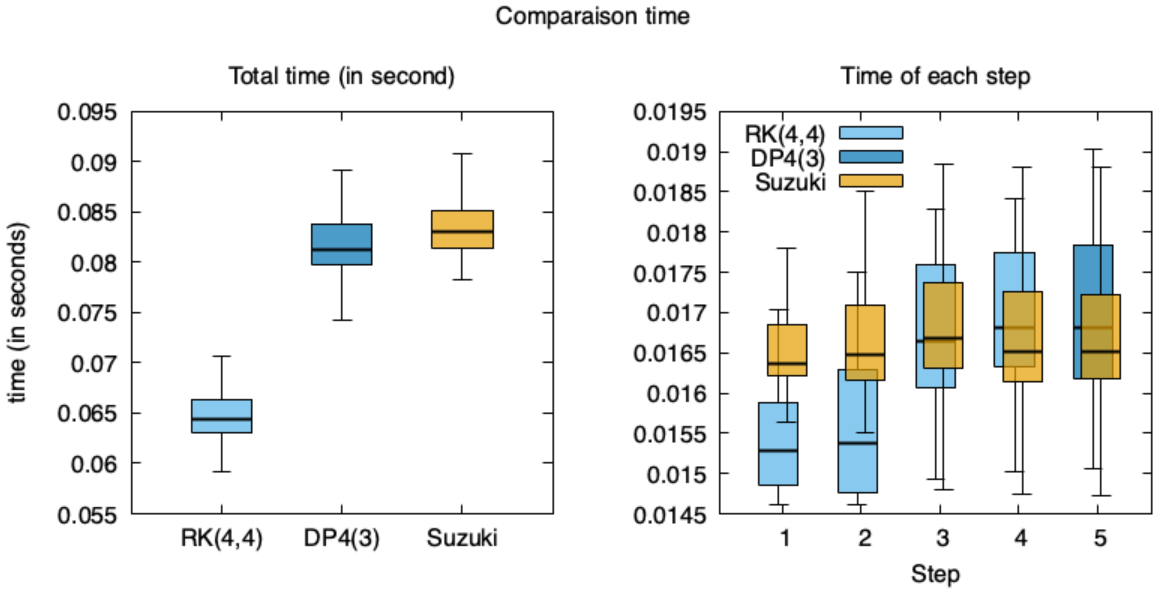

Figure 11: Mean value and quartiles of computational time for one iteration (Left) and each step of one iteration (Right).

5 Vlasov hybrid model: $1dz$-$3dv$ case

This section is dedicated to the study of the numerical methods discussed above (Hamiltonian splitting and Lawon) on a more complex and realistic four dimensional problem. Due to the high dimensionality of the problem, we will not consider the full kinetic problem as in the previous section but we will discuss some specific modifications of the numerical methods which are required to make four dimensional simulations efficient.

As in [1], starting from the full six-dimensional hybrid problem (2)-(5), we consider here the case of a wave propagation parallel to a uniform magnetic field $\mathbf{B}_0(\mathbf{x}) = B_0\mathbf{e}_z = (0, 0, B_0)^T, B_0 > 0$ and $\Omega_{pe}^2 = 4$ so that the wave vector $\mathbf{k} = k\mathbf{e}_z = (0, 0, k)^T$ and the problem becomes one dimensional in space but the three dimensions in velocity are kept.

Thus, we consider the following unknown for the VHL

$$f_h(t,z,\mathbf{v}), E_x(t,z), E_y(t,z), B_x(t,z), B_y(t,z), j_{c,x}(t,z), j_{c,y}(t,z),$$

with $\mathbf{v} = (v_x, v_y, v_z)$ and$j_{c,x/y} = -\rho_c^{(0)} u_{c,x/y}$. The model is normalized as in [1] and reads as

$$\frac{\partial j_{c,x}}{\partial t} = \Omega_{pe}^2 E_x - j_{c,y} B_0, \tag{38}$$

$$\frac{\partial j_{c,y}}{\partial t} = \Omega_{pe}^2 E_y + j_{c,x} B_0, \tag{39}$$

$$\begin{aligned}\frac{\partial f_h}{\partial t} + v_z \partial_z f_h - (E_x + v_y B_0 - v_z B_y)\, \partial_{v_x} f_h \\ - (E_y - v_x B_0 + v_z B_x)\, \partial_{v_y} f_h - (v_x B_y - v_y B_x)\, \partial_{v_z} f_h = 0,\end{aligned} \tag{40}$$

$$\frac{\partial B_x}{\partial t} = \partial_z E_y, \tag{41}$$

$$\frac{\partial B_y}{\partial t} = -\partial_z E_x, \tag{42}$$

$$\frac{\partial E_x}{\partial t} = -\partial_z B_y - j_{c,x} + \int v_x f_h \,\mathrm{d}\mathbf{v}, \tag{43}$$

$$\frac{\partial E_y}{\partial t} = \partial_z B_x - j_{c,y} + \int v_y f_h \,\mathrm{d}\mathbf{v}. \tag{44}$$

Let us detail the Poisson bracket in this context. First, the Hamiltonian reduces to (we denote $\mathbf{B} := (B_x, B_y, 0)^\mathsf{T}$)

$$\mathcal{H} = \underbrace{\frac{1}{2}\int_{\mathbb{R}} (E_x^2 + E_y^2)\,\mathrm{d}z}_{\mathcal{H}_E} + \underbrace{\frac{1}{2}\int_{\mathbb{R}} (B_x^2 + B_y^2)\,\mathrm{d}z}_{\mathcal{H}_B} + \underbrace{\frac{1}{2}\int_{\mathbb{R}} \frac{1}{\Omega_{pe}^2}(j_{c,x}^2 + j_{c,y}^2)\,\mathrm{d}z}_{\mathcal{H}_{j_c}} + \underbrace{\frac{1}{2}\int_{\mathbb{R}}\int_{\mathbb{R}^3} |\mathbf{v}|^2 f \,\mathrm{d}z\mathrm{d}\mathbf{v}}_{\mathcal{H}_{f_h}}. \tag{45}$$

We define one bracket as follows, for two given functionals $\mathcal{F}, \mathcal{G}$ of the unknown

$$\begin{aligned}\{\mathcal{F},\mathcal{G}\}[j_{c,x}, j_{c,y}, B_x, B_y, E_x, E_y, f_h] &= \int_{\mathbb{R}}\int_{\mathbb{R}^3} f_h \left(\partial_z \frac{\delta \mathcal{F}}{\delta f_h}\partial_{v_z}\frac{\delta \mathcal{G}}{\delta f_h} - \partial_{v_z}\frac{\delta \mathcal{F}}{\delta f_h}\partial_z \frac{\delta \mathcal{G}}{\delta f_h}\right)\mathrm{d}\mathbf{v}\mathrm{d}z \\ &+ \int_{\mathbb{R}}\int_{\mathbb{R}^3} f_h \left(\partial_{v_x}\frac{\delta \mathcal{F}}{\delta f_h}\frac{\delta \mathcal{G}}{\delta E_x} + \partial_{v_y}\frac{\delta \mathcal{F}}{\delta f_h}\frac{\delta \mathcal{G}}{\delta E_y} - \partial_{v_x}\frac{\delta \mathcal{G}}{\delta f_h}\frac{\delta \mathcal{F}}{\delta E_x} - \partial_{v_y}\frac{\delta \mathcal{G}}{\delta f_h}\frac{\delta \mathcal{F}}{\delta E_y}\right)\mathrm{d}\mathbf{v}\mathrm{d}z \\ &+ \int_{\mathbb{R}}\int_{\mathbb{R}^3} f_h(\mathbf{B}+\mathbf{B}_0)\cdot\left(\nabla_{\mathbf{v}}\frac{\delta \mathcal{F}}{\delta f_h}\times\nabla_{\mathbf{v}}\frac{\delta \mathcal{G}}{\delta f_h}\right)\mathrm{d}\mathbf{v}\mathrm{d}z \\ &+ \int_{\mathbb{R}} \left(-\partial_z\frac{\delta \mathcal{F}}{\delta E_y}\frac{\delta \mathcal{G}}{\delta B_x} + \partial_z\frac{\delta \mathcal{F}}{\delta E_x}\frac{\delta \mathcal{G}}{\delta B_y} + \partial_z\frac{\delta \mathcal{G}}{\delta E_y}\frac{\delta \mathcal{F}}{\delta B_x} - \partial_z\frac{\delta \mathcal{G}}{\delta E_x}\frac{\delta \mathcal{F}}{\delta B_y}\right)\mathrm{d}z \\ &+ \int_{\mathbb{R}} \Omega_{pe}^2\left(\frac{\delta \mathcal{F}}{\delta j_{c,x}}\frac{\delta \mathcal{G}}{\delta E_x} + \frac{\delta \mathcal{F}}{\delta j_{c,y}}\frac{\delta \mathcal{G}}{\delta E_y} - \frac{\delta \mathcal{G}}{\delta j_{c,x}}\frac{\delta \mathcal{F}}{\delta E_x} - \frac{\delta \mathcal{G}}{\delta j_{c,y}}\frac{\delta \mathcal{F}}{\delta E_y}\right)\mathrm{d}z \\ &+ \int_{\mathbb{R}} \Omega_{pe}^2 B_0\left(\frac{\delta \mathcal{F}}{\delta j_{c,x}}\frac{\delta \mathcal{G}}{\delta j_{c,y}} - \frac{\delta \mathcal{F}}{\delta j_{c,y}}\frac{\delta \mathcal{G}}{\delta j_{c,x}}\right)\mathrm{d}z.\end{aligned} \tag{46}$$

From this, one can rewrite the system (38)-(44) as

$$\partial_t U = \{U, \mathcal{H}\},$$

with $U(t,z,\mathbf{v}) = (j_{c,\perp}(t,z), B_\perp(t,z), E_\perp(t,z), f_h(t,z,\mathbf{v})$ where $\mathcal{H}$ is given by (45) and $j_{c,\perp} = (j_{c,x}, j_{c,y})^\mathsf{T}, E_\perp = (E_x, E_y)^\mathsf{T}, B_\perp = (B_x, B_y)^\mathsf{T}$. In the rest of this section, we will also use the notation $v_\perp = (v_x, v_y)^\mathsf{T} \in \mathbb{R}^2$ such that $\mathbf{v} = (v_\perp, v_z)^\mathsf{T}$ and we introduce the symplectic matrix

$$J = \begin{pmatrix} 0 & 1 \\ -1 & 0 \end{pmatrix}.$$

5.1 Numerical schemes

In this part, we will present some modifications of the Hamiltonian splitting and Lawson methods which are specific to the numerical resolution of the $1dz - 3dv$ hybrid model.

5.1.1 Hamiltonian splitting

As in the previous section, we adapt a Hamiltonian splitting method to our case in which the Hamiltonian (45) can be split into four parts. The *splitting* can be deduced from (45) through

$$\partial_t U = \{U, \mathcal{H}_E\} + \{U, \mathcal{H}_B\} + \{U, \mathcal{H}_{j_c}\} + \{U, \mathcal{H}_{f_h}\}, \quad U(t=0) = U_0. \tag{47}$$

In the sequel, we will compute $\varphi_t^{[E]}$, $\varphi_t^{[B]}$, $\varphi_t^{[j_c]}$ and $\varphi_t^{[f_h]}$ the solutions corresponding to each part so that the solution $\varphi(U_0)$ of (47) can be approximated at time t with a composition of the subflows $\varphi_t^{[E,B,j_c,f_h]}$.

Part $\mathcal{H}_E$

To compute the solution of the subflow corresponding to $\mathcal{H}_\mathbf{E}$, we have to solve the following system

$$\partial_t E_\perp = (0,0)^\mathsf{T}, \partial_t f_h - E_\perp \cdot \nabla_{v_\perp} f_h = 0, \partial_t B_\perp = J\partial_z E_\perp, \partial_t j_{c,\perp} = \Omega_{pe}^2 E_\perp.$$

Starting with the initial condition $U(t=0) = U_0 = (j_{c,\perp}, E_\perp, B_\perp, f_h)(t=0)$, the solution at time t is

$$\varphi_t^{[E]}(U_0) = \begin{pmatrix} j_{c,\perp}(0) + t\Omega_{pe}^2 E_\perp(0) \\ E_\perp(0) \\ B_\perp(0) + tJ\partial_z E_\perp(0) \\ f_h(0, z, v_\perp + tE_\perp(0), v_z) \end{pmatrix}.$$

The computation of $f_h(0, z, v_\perp + tE_\perp(0), v_z)$ is performed using two one-dimensional interpolations (in v_x and v_y) of fifth order Lagrange type.

Part $\mathcal{H}_B$

Now we compute $\varphi_t^{[B]}$ the solution to

$$\partial_t(f_h, B_\perp, j_{c,\perp}) = 0, \partial_t E_\perp = -J\partial_z B_\perp.$$

We obtain

$$\varphi_t^{[B]}(U_0) = \begin{pmatrix} j_{c,\perp}(0) \\ E_\perp(0) - tJ\partial_z B_\perp(0) \\ B_\perp(0) \\ f_h(0) \end{pmatrix}.$$

Part $\mathcal{H}_{j_c}$

Here we compute $\varphi_t^{[j_c]}$ the solution to

$$\partial_t(f_h, B_\perp) = 0, \partial_t E_\perp = -j_{c,\perp}, \partial_t j_{c,\perp} = -J j_{c,\perp} B_0.$$

We then have

$$\varphi_t^{[j_c]}(U_0) = \begin{pmatrix} \exp(-Jt) j_{c,\perp}(0) B_0, \\ E_\perp(0) - J\Big(\exp(-Jt) - I\Big) j_{c,\perp}(0) \\ B_\perp(0) \\ f_h(0) \end{pmatrix},$$

since $\int_0^t \exp(-Js)) j_{c,\perp}(0)\,\mathrm{d}s = J\Big(\exp(-Jt) - I\Big) j_{c,\perp}(0)$.

Part $\mathcal{H}_{f_h}$

For this last part, we have to compute the solution to

$$\partial_t(B_\perp, j_{c,\perp}) = 0,$$
$$\partial_t f_h + v_z\partial_z f_h - (v_y B_0 - v_z B_y)\,\partial_{v_x} f_h - (-v_x B_0 + v_z B_x)\,\partial_{v_y} f_h - (v_x B_y - v_y B_x)\,\partial_{v_z} f_h = 0,$$
$$\partial_t E_\perp = \int v_\perp f_h\,\mathrm{d}\mathbf{v}.$$

As in the Vlasov-Maxwell case (see [9]), this system can not be solved exactly in time but following [9], we split again the Hamiltonian $\mathcal{H}_{f_h}$ into $\mathcal{H}_{f_h} = \mathcal{H}_{f_h,x} + \mathcal{H}_{f_h,y} + \mathcal{H}_{f_h,z}$ where $\mathcal{H}_{f_h,i} = \frac{1}{2}\int v_i^2 f_h\,\mathrm{d}\mathbf{v}, i = x, y, z$. Then, it leads to the following subsystems

- $\mathcal{H}_{f_h,x}$: $\partial_t(B_\perp, j_{c,\perp}, E_y) = 0$, $\partial_t f_h - \big(-v_x B_0\partial_{v_y} f_h + B_y v_x \partial_{v_z} f_h\big) = 0$, $\partial_t E_x = \int v_x f_h\,\mathrm{d}\mathbf{v}$. We first remark that $\int v_x f_h\,\mathrm{d}\mathbf{v}$ is constant in time so that the Ampère equation can be solved easily. Moreover, the transport equation can be solved exactly using a directional splitting since the two operators commute. Then, we have

$$\varphi_t^{[f_h,x]}(U_0) = \begin{pmatrix} j_{c,\perp}(0) \\ E_x(0) + t\int v_x f_h(0)\,\mathrm{d}\mathbf{v} \\ E_y(0) \\ B_\perp(0) \\ f_h(0, z, v_x, v_y - tv_x B_0, v_z + tB_y v_x) \end{pmatrix}.$$

  In practice, two one-dimensional interpolations are performed (using fifth order Lagrange).

- $\mathcal{H}_{f_h,y}$: $\partial_t(B_\perp, j_{c,\perp}, E_x) = 0$, $\partial_t f_h - (B_0 v_y \partial_{v_x} f_h - B_x v_y \partial_{v_z} f_h) = 0$, $\partial_t E_y = \int v_y f_h \, \mathrm{d}\mathbf{v}$. This step is very similar to the previous one and we have

$$\varphi_t^{[f_h,y]}(U_0) = \begin{pmatrix} j_{c,\perp}(0) \\ E_x(0) \\ E_y(0) + t \int v_y f_h(0) \, \mathrm{d}\mathbf{v} \\ B_\perp(0) \\ f_h(0, z, v_x + t v_y B_0, v_y, v_z - t B_x v_y) \end{pmatrix}.$$

  In practice, two one-dimensional interpolations are performed (using fifth order Lagrange).

- $\mathcal{H}_{f_h,z}$: $\partial_t(B_\perp, j_{c,\perp}, E_\perp) = 0$, $\partial_t f_h + v_z \partial_z f_h - \left(-B_y v_z \partial_{v_x} f_h + v_z B_x \partial_{v_y} f_h\right) = 0$.

The calculation of the $\mathcal{H}_{f_h,z}$ part deserves more attention. First, we introduce a new function $g(t, z, \mathbf{v}) := f(t, z + t v_z, \mathbf{v})$ which satisfies

$$\partial_t g + B_y(0, z + t v_z) v_z \partial_{v_x} g - v_z B_x(0, z + t v_z) \partial_{v_y} g = 0. \tag{48}$$

It turns out that this transport equation can be solved exactly in time and the details are given in the following. First, we observe that the characteristics of (48) can be solved exactly

$$\dot{v}_x(t) = B_y(0, z(0) + t v_z(0)) v_z(0), \quad \dot{v}_y(t) = -B_x(0, z(0) + t v_z(0)) v_z(0). \tag{49}$$

Even if z, v_z and $B_{x,y}$ are constant in time during this step, the filtering has introduced a time dependency. This can be overcome by expanding the magnetic field $B_\perp$ into Fourier series in the z variable, which leads to

$$B_\perp(t, z) = B_\perp(0, z) = \sum_k \hat{B}_\perp(0, k) e^{ikz}, \text{ so that } B_\perp(0, z + t v_z) = \sum_k \hat{B}_\perp(0, k) e^{ik(z + t v_z)}.$$

Then, integrating in time the first equation of (49), we have

$$\begin{aligned} v_x(t) &= v_x(0) + v_z(0) \int_0^t \sum_k \hat{B}_y(0, k) e^{ik(z(0) + s v_z(0))} \, \mathrm{d}s \\ &= v_x(0) + v_z(0) \sum_k \hat{B}_y(0, k) e^{ikz(0)} \int_0^t e^{iksv_z(0)} \, \mathrm{d}s \\ &= v_x(0) + \sum_k \hat{B}_y(0, k) \frac{1}{ik} e^{ikz(0)} (e^{iktv_z(0)} - 1), \end{aligned}$$

whereas for the equation on v_y, we have

$$\begin{aligned} v_y(t) &= v_y(0) - v_z(0) \int_0^t \sum_k \hat{B}_x(0, k) e^{ik(z(0) + s v_z(0))} \, \mathrm{d}s \\ &= v_y(0) - \sum_k \hat{B}_x(0, k) \frac{1}{ik} e^{ikz(0)} (e^{iktv_z(0)} - 1). \end{aligned}$$

Then, the dynamics of $\mathcal{H}_{f_h,z}$ is given by

$$g(t,z,\mathbf{v}) = g\left(0, z, v_x - \sum_k \hat{B}_y(0,k)\frac{1}{ik}e^{ikz}(e^{iktv_z}-1), \right.$$
$$\left. v_y + \sum_k \hat{B}_x(0,k)\frac{1}{ik}e^{ikz}(e^{iktv_z}-1), v_z\right).$$

Finally, $f_h(t)$ is obtained by performing the inverse change of unknown

$$f(t,z,\mathbf{v}) = g(t, z - tv_z, \mathbf{v}).$$

Then, the $\mathcal{H}_{f_h,z}$ part can be solved exactly in time using three one-dimensional linear advections (still performed using fifth order Lagrange interpolation). To conclude, the solution of the $\mathcal{H}_{f_h}$ part can be done using the composition of the $\mathcal{H}_{f_h,x}, \mathcal{H}_{f_h,y}$ and $\mathcal{H}_{f_h,z}$ parts.

5.1.2 Exponential integrators

In this part, we present the exponential integrators to discretize in time the VHL (38)-(44). Indeed, as mentioned above, the exponential of the whole linear part is complex or costly to evaluate. Hence, we propose here some modifications compared to the Lawson scheme presented in Subsection 3.2 based on the two guidelines: we want to remove the most restrictive stability conditions and we want to consider a linear part whose exponential is efficient to evaluate.

In this spirit, we first observe that the term $(\mathbf{v}\times\mathbf{B}_0)$ induces a restrictive CFL conditions which can be overcome by performing the following change of variables $w = \exp(tB_0J)v$ (with $w = (w_x, w_y)^\mathsf{T}$ and $v = (v_x, v_y)^\mathsf{T}$) to filter out this term with very slight influence on the rest of the system. Then, we introduce $g(t,z,w,v_z) = f_h(t,z,\exp(-tB_0J)w, v_z)$ with

$$\exp(-tB_0J) = \begin{pmatrix} \cos(tB_0) & -\sin(tB_0) \\ \sin(tB_0) & \cos(tB_0)\end{pmatrix}, \quad J = \begin{pmatrix} 0 & 1 \\ -1 & 0\end{pmatrix},$$

so that $\exp(-tB_0J)w = (\cos(tB_0)w_x - \sin(tB_0)w_y, \sin(tB_0)w_x + \cos(tB_0)w_y)^\mathsf{T}$. Hence, we derive the equation on g

$$\partial_t g + v_z\partial_z g - e^{-tB_0J}E_\perp\cdot\nabla_w g - \mathcal{B}g = 0, \tag{50}$$

where $\mathcal{B}g$ is given by

$$\begin{aligned}\mathcal{B}g &:= (\mathbf{v}\times\mathbf{B})\cdot\nabla_{\mathbf{v}} f_h \\ &= \begin{pmatrix} \cos(tB_0)w_x - \sin(tB_0)w_y \\ \sin(tB_0)w_x + \cos(tB_0)w_y \\ v_z\end{pmatrix} \times \begin{pmatrix} B_x \\ B_y \\ 0\end{pmatrix} \cdot \begin{pmatrix} e^{-tB_0J}\nabla_w g \\ \partial_{v_z} g\end{pmatrix} \\ &= \begin{pmatrix} v_z(-\cos(tB_0)B_y + \sin(tB_0)B_x) \\ v_z(\sin(tB_0)B_y + \cos(tB_0)B_x) \\ (\cos(tB_0)w_x - \sin(tB_0)w_y)B_y - (\sin(tB_0)w_x + \cos(tB_0)w_y)B_x\end{pmatrix}\cdot\begin{pmatrix}\partial_{w_x} g \\ \partial_{w_y} g \\ \partial_{v_z} g\end{pmatrix}\end{aligned} \tag{51}$$

For the Ampère equation (43)-(44), the integrals have to be recast in the new variables

$$\int v f \, \mathrm{d}\mathbf{v} = \int (e^{-tB_0 J} w) g \, \mathrm{d}w \mathrm{d}v_z,$$

so that they can be rewritten as

$$\partial_t E_\perp = -J \partial_z B_\perp - j_{c,\perp} + \int (e^{-tB_0 J} w) g \, \mathrm{d}w \mathrm{d}v_z. \tag{52}$$

The rest of the equations is unchanged.

The second modification is based on the fact the exponential of the linear part (even with the previous filtering step) turns out to be quite complicated and in practice too costly, even using formal languages. Then, we propose to transfer from the linear part the space derivatives of the Maxwell equations to include them in the nonlinear part so that the exponential of the linear part is easier to evaluate. We then reformulate the system as

$$\partial_t U + AU + F(t, U) = 0,$$

with the following linear part

$$AU = \begin{pmatrix} 0 & B_0 & 0 & 0 & -\Omega_{pe}^2 & 0 & 0 \\ -B_0 & 0 & 0 & 0 & 0 & -\Omega_{pe}^2 & 0 \\ 0 & 0 & 0 & 0 & 0 & 0 & 0 \\ 0 & 0 & 0 & 0 & 0 & 0 & 0 \\ 1 & 0 & 0 & 0 & 0 & 0 & 0 \\ 0 & 1 & 0 & 0 & 0 & 0 & 0 \\ 0 & 0 & 0 & 0 & 0 & 0 & v_z \partial_z \end{pmatrix} U,$$

and with the following nonlinear part

$$F(t, U) = \begin{pmatrix} 0 \\ 0 \\ -\partial_z E_y \\ \partial_z E_x \\ \partial_z B_y - \int_{\mathbb{R}^3} (\cos(tB_0) w_x - \sin(tB_0) w_y) g \, \mathrm{d}w \mathrm{d}v_z \\ -\partial_z B_x - \int_{\mathbb{R}^3} (\sin(tB_0) w_x + \cos(tB_0) w_y) g \, \mathrm{d}w \mathrm{d}v_z \\ -e^{-tB_0 J} E_\perp \cdot \nabla_w g - \mathcal{B} g \end{pmatrix} \tag{53}$$

In return for an easy computation of e^{tA}, we now have CFL stability condition coming from the Maxwell equations in the nonlinear term.

Then, a standard exponential integrator can be used by simply considering Fourier transform in space whereas WENO methods will be used to approximate the velocity derivative. Note that the change of variables induces a time dependency on the nonlinear term (which was not the case in the $1dx - 1dv$ case).

5.2 Numerical results

In this part, we present some numerical results for the $1dz - 3dv$ hybrid model obtained with the numerical methods presented above. Following [1], we consider the following initial condition

$$f_h(t=0,z,\mathbf{v}) = \frac{\rho_h}{(2\pi)^{3/2}\bar{v}_\parallel \bar{v}_\perp^2} \exp\Big(- \frac{v_z^2}{2\bar{v}_\parallel^2} - \frac{(v_x^2+v_y^2)}{2\bar{v}_\perp^2}\Big),$$

with $z \in [0, 2\pi/k], k = 2$, $\bar{v}_\parallel = 0.2, \bar{v}_\perp = 0.6$, $\rho_h = 0.2$ and $B_x(t=0,z) = \epsilon \sin(kz)$, the other unknown $(E_x, E_y, j_{c,x}, j_{c,y}, B_y)$ are zero initially. The velocity domain is truncated to $\mathbf{v} = [-3.6, 3.6] \times [-3.6, 3.6] \times [-2.4, 2.4]$ and we denote $N_x, N_{v_x}, N_{v_y}, N_{v_z}$ the number of points in each direction.

We are interested in the time history of the following energies (magnetic energy, electric energy, energy of the cold and hot particles)

$$\begin{aligned}
\mathcal{H}_B(t) &= \frac{1}{2}\int (B_x^2(t,z) + B_y^2(t,z))\,\mathrm{d}z, \quad \mathcal{H}_E(t) = \frac{1}{2}\int (E_x^2(t,z) + E_y^2(t,z) + E_z^2(t,z))\,\mathrm{d}z, \\
\mathcal{H}_c(t) &= \frac{1}{2\Omega_{pe}^2}\int (j_{c,x}^2(t,z) + j_{c,y}^2(t,z))\,\mathrm{d}z, \quad \mathcal{H}_h(t) = \frac{1}{2}\iint |\mathbf{v}|^2 f_h(t,z,\mathbf{v})\,\mathrm{d}\mathbf{v}\mathrm{d}z,
\end{aligned}$$

whose sum is preserved with time

$$\frac{\mathrm{d}\mathcal{H}}{\mathrm{d}t} = \frac{\mathrm{d}(\mathcal{H}_B + \mathcal{H}_E + \mathcal{H}_c + \mathcal{H}_h)}{\mathrm{d}t} = 0.$$

We first consider both Lawson and splitting methods with fixed time step (as presented in Subsection 5.1): two Lawson methods (Lawson-RK(4, 4) and Lawson-RK(3, 3)) and two splitting methods (Lie and Strang). We will not present results from the Suzuki schemes since it mainly gives the same results as Strang and it costs five times the Strang method. Indeed, when a splitting method involves a lot of subparts (seven in our case), the number of stages required to reach high order accuracy increases dramatically (even if some strategies can be used to avoid this (see [14])). To give an example, Strang splitting requires 15 stages so that Suzuki requires $5 \times 15 = 75$ stages per iteration which is clearly too much in the high dimensional kinetic context and which makes Suzuki less attractive. On the contrary, Lawson methods turn out to be a good compromise since they are optimal in the sense that they involve as many stages as their order. For Vlasov type systems, this is of crucial importance. Moreover, Lawson methods are versatile since the linear part can be chosen in order to overcome some specific constraints of the model: the complexity of the exponential part evaluation, the presence of a term involving a stringent CFL condition... Moreover, filtering out the term $\mathbf{v} \times \mathbf{B}_0$ is also an important feature of our Lawson integrators since it enables to take into account this rotation term analytically and to remove the associated CFL condition. Let us remark that a similar filtering strategy may have been used within the splitting framework but it leads to additional steps in the $\mathcal{H}_{f_h}$ subpart which is already the most costly one.

Since the Maxwell equations are approximated in time using explicit schemes, this still induces a CFL condition on the two approaches (Lawson and splitting) as discussed

in [32]. Indeed, focusing only on the unknown (E_x, E_y, B_x, B_y), it is possible to compute the stability condition on the time step Δt as a function of the space mesh Δz. The CFL conditions are gathered in Table 4. For Lawson methods, another CFL condition coming

methods	CFL condition
Lie	$(\sqrt{2}/\pi)\Delta z$
Strang	$(2/\pi)\Delta z$
Lawson-RK(3, 3)	$(\sqrt{3}/\pi)\Delta z$
Lawson-RK(4, 4)	$(2\sqrt{2}/\pi)\Delta z$

Table 4: CFL condition from the Maxwell part using the different time integrators.

from the velocity discretization is also present but the condition from Maxwell equations is the most restrictive one. Let us remark that it would be possible to remove it by incorporating the Maxwell equations in the linear part (as presented in (13) in Section 3.2). However, as discussed above, the calculation of the exponential of the matrix (13) is complicated and more advanced techniques are required to evaluate it, like the use of Padé approximant; this will be the topic of a future work.

In Figure 12, we plot the time history of the electric energy, the magnetic energy and the energy of cold particles defined in (54), in semi-log scale for the Strang and Lawson-RK(3, 3) methods. We have chosen a coarse mesh $27 \times 32 \times 32 \times 41$, $\Delta t = 0.05$. We have considered a small perturbation $\epsilon = 10^{-5}$ in order to observe a long linear phase (up to $t \approx 100$) whereas the nonlinear phase is developing up to the final time $t = 200$. For the linear phase, it is possible to compare the numerical results with the solution of the dispersion relation from [1]. First, as expected, the three energies grows exponentially which traduces the fact that some energy is transferred from the fast particles to the electromagnetic fields and to the cold particles. After this linear phase, the fields amplitude saturates, which means that the nonlinear terms start to play a significative role, so that the linear theory is not valid anymore. First we observe that the two methods are able to capture the underlying phenomena and a very good agreement with the instability rate computed from the linear theory is observed. Moreover, the saturation is also very similar for the two methods.

In Figure 12, we show the total energy conservation as a function of time for the two methods (Strang and Lawson-RK(3, 3)). Even if the phase space mesh is coarse, the total energy is quite well preserved: about 8% for Lawson method and about 5% for Strang splitting methods. As expected (and as observed in the $1dx - 1dv$ case), Hamiltonian splittings based methods have a good behavior on this diagnostics. However, the effect of the coarse mesh makes the results of Strang not as good as in the $1dx - 1dv$ case for which the mesh was refined. Moreover, let us recall that the cost of Strang is more important than the one of Lawson-RK(3, 3) in this four-dimensional context: Strang is almost twice more costly as Lawson-RK(3, 3).

Then, we investigate the effect of the filtering of the term $\mathbf{v} \times \mathbf{B}_0$ in the Lawson schemes. In Figure 14, we show the time history of the electric energy (in semi-log scale) obtained by the two versions of Lawson schemes (filtered and non-filtered) using two different phase-space meshes ($15 \times 20 \times 20 \times 41$ and $15 \times 32 \times 32 \times 41$) with $\Delta t = 0.1$.

One can observe the impact of the refinement in the $v_\perp$ direction on the non-filtered version whereas the filtered version has the good instability rate even with a coarse mesh.

Hence, for the last test, we only consider Lawson methods and look at the robustness of the adaptive Lawson-DP4(3) method. This approach is interesting since (i) in the linear phase electromagnetic fields are small so that the stability condition coming from the nonlinear part of the equations is not restrictive; (ii) in the nonlinear phase, the local error estimator of the embedded Runge-Kutta method will ensure stability automatically. In practice, due to space derivatives in (53), stability condition is still restrictive, so that (i) is not fully satisfied. In the following, we consider $N_z = 27, N_{v_x} = 32, N_{v_y} = 32, N_{v_z} = 41$, $\text{tol} = 6 \times 10^{-5}$ and the time step is computed as

$$\Delta t_0 = \frac{C}{2}\Delta z, \quad \Delta t_{n+1} = \min\left(\max\left(\sqrt[p]{\frac{\text{tol}}{L_{[p]}^{n+1}}}\Delta t_n, \frac{C}{2}\Delta z\right), 3C\Delta z\right), n \geq 0, \tag{54}$$

where $L_{[p]}^{n+1}$ is the local error given by (15) and C is given from Table 4. Note that we imposed the upper bound $3C\Delta z$ in order to avoid large time steps and then large errors that may occur at the very beginning of the simulation. In Figure 15, the time history of the electric energy is shown. In Figure 16, the history of the time steps (top) and of the local error (bottom) are presented. In simulation with Lawson-DP4(3), the time step is initialized to $\Delta t_0 = \frac{1}{2}\frac{2\sqrt{2}}{N_z} \approx 0.05$, we can see that the next three iterations used $\Delta t_n = 3\frac{2\sqrt{2}}{N_z} \approx 0.3$ which is the upper bound of (54); this comes from the fact that the electromagnetic fields are very small and the local error is very small as well. All the other iterations use a time step close to the stability condition coming from Maxwell equations i.e. $\Delta t_n \approx \frac{2\sqrt{2}}{N_z}$. It is worth mentioning that the adaptive time step strategy automatically finds this optimal time step (the adaptive stepping even overestimates the CFL for 16% of succeeded iterations). Unlike in the $1dx - 1dv$ problem in which 95.8% of iterations are accepted, in this $1dx - 3dv$ problem only 71% of iterations are accepted.

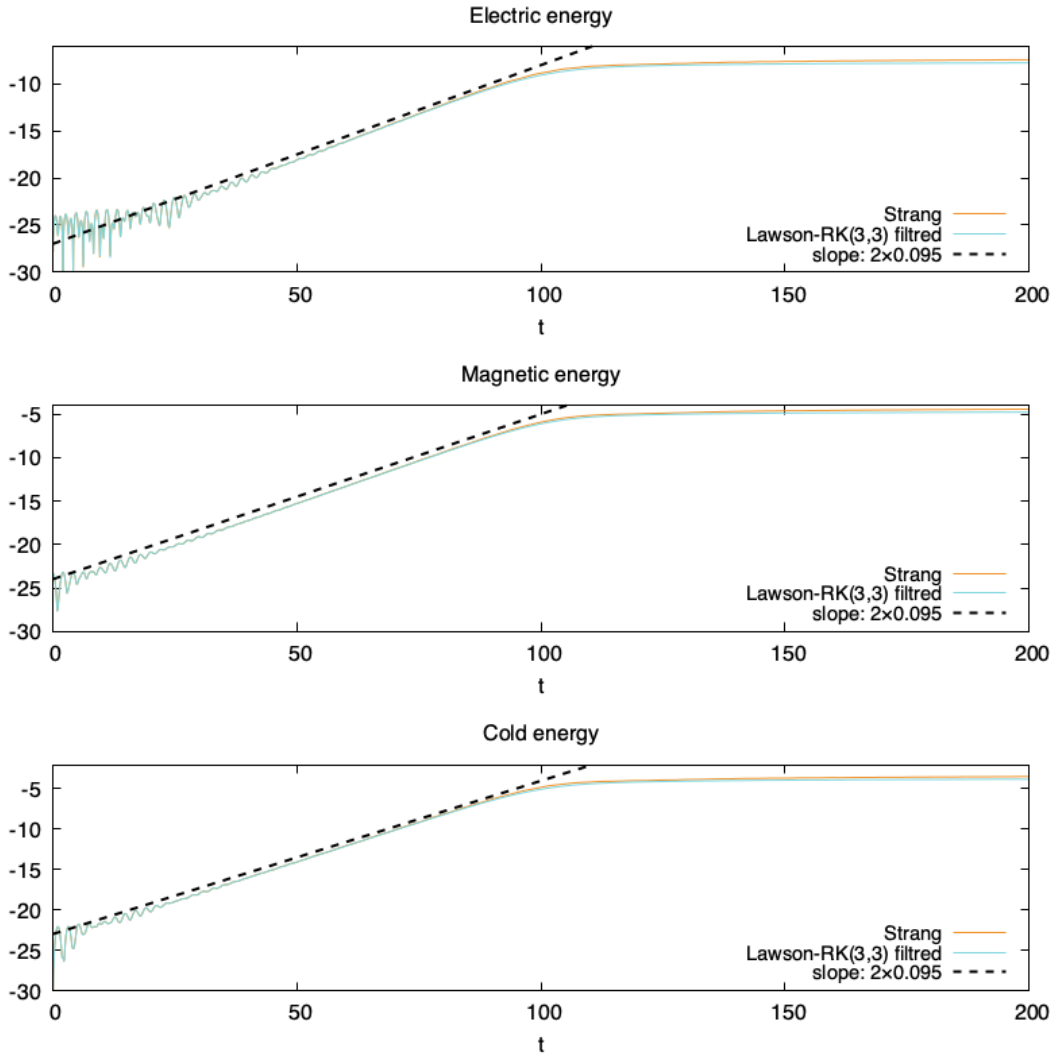

Figure 12: Time evolution of the electric energy, the magnetic energy and the energy of cold particles defined in (54), in semi-log scale for Strang and Lawson-RK(3, 3). $\Delta t = 0.05, N_z = 27, N_{v_x} = 32, N_{v_y} = 32, N_{v_z} = 41$.

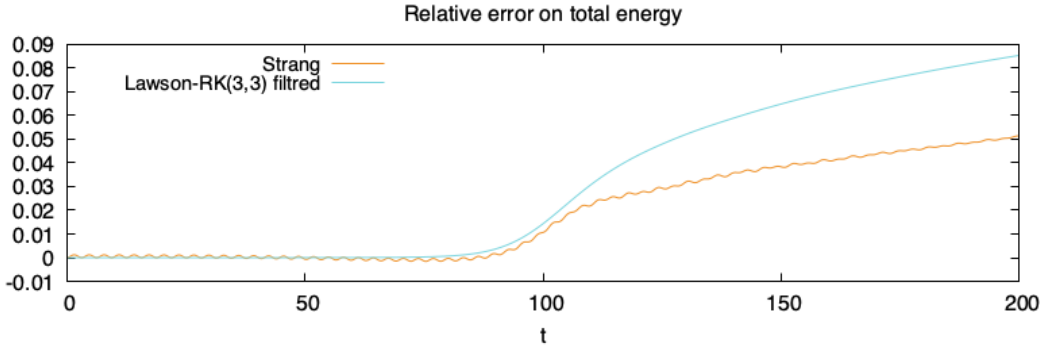

Figure 13: Time evolution of the total energy for Strang and Lawson-RK(3, 3). $\Delta t = 0.05, N_z = 27, N_{v_x} = 32, N_{v_y} = 32, N_{v_z} = 41$.

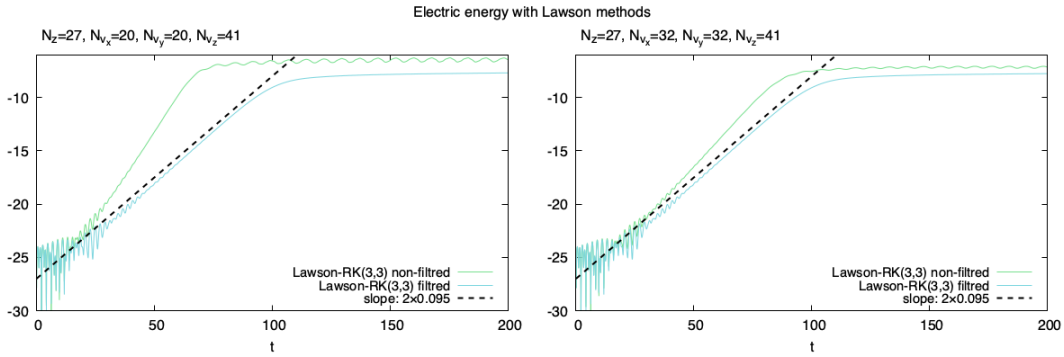

Figure 14: Time evolution of the electric energy for the filtered and unfiltered versions of Lawson-RK(3, 3). Left: $\Delta t = 0.05, N_z = 27, N_{v_x} = 20, N_{v_y} = 20, N_{v_z} = 41$. Right: $\Delta t = 0.05, N_z = 27, N_{v_x} = 32, N_{v_y} = 32, N_{v_z} = 41$

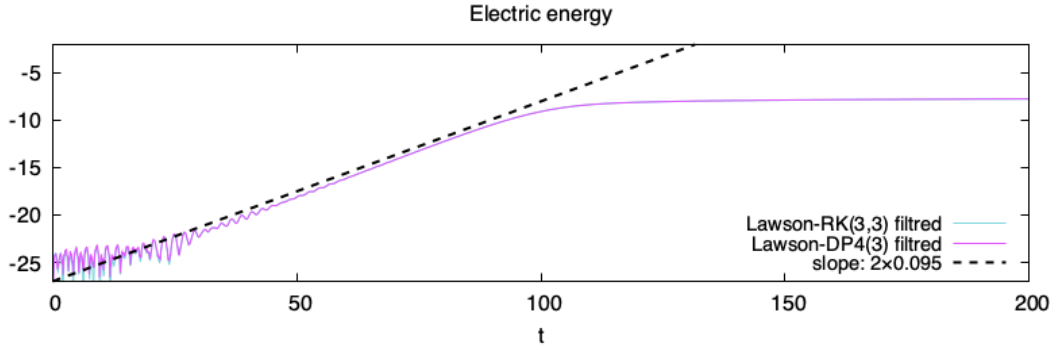

Figure 15: Time evolution of the electric energy defined in (54), in semi-log scale for Lawson-RK(3, 3) ($\Delta t = 0.05$) and Lawson-DP4(3). $N_z = 27, N_{v_x} = 32, N_{v_y} = 32, N_{v_z} = 41$.

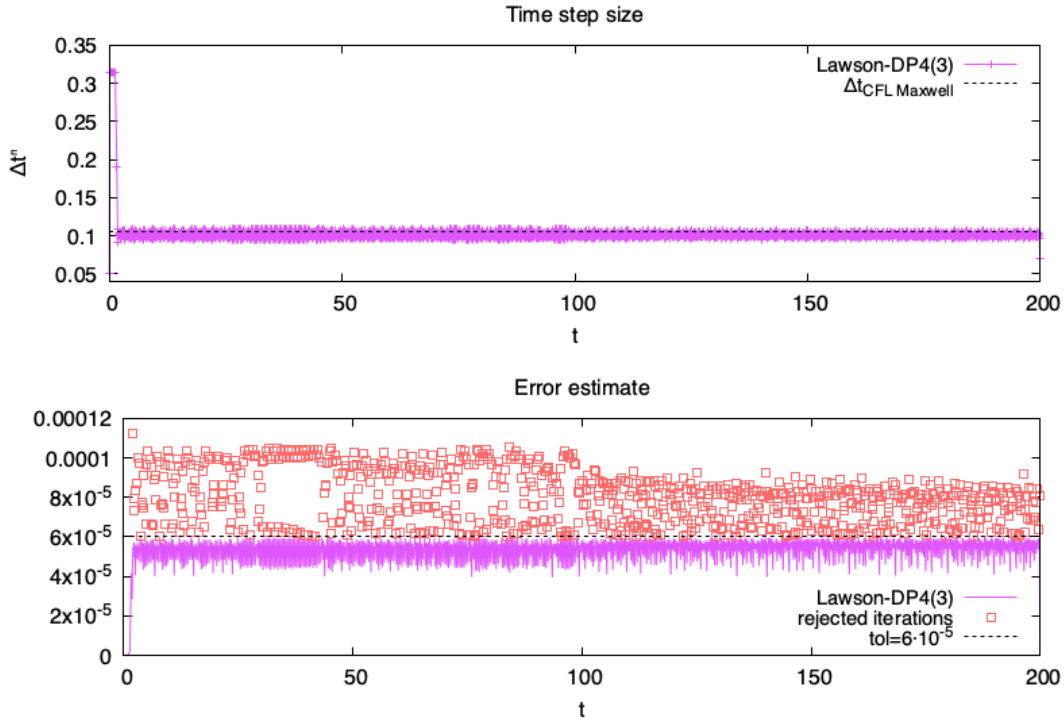

Figure 16: Time evolution of the time step (top) and the local error (bottom) for Lawson-DP4(3). $N_z = 27, N_{v_x} = 32, N_{v_y} = 32, N_{v_z} = 41$.

6 Conclusion

In this work, we investigate the performances of two different time integrators coupled with Eulerian methods for a hybrid fluid-kinetic model. This hybrid model, for which we derive the Hamiltonian structure (Poisson bracket and Hamiltonian) intends to describe electrons plasma which can be divided into two populations: a cold part described with a linearized fluid model and a hot part described through a kinetic model. First, we study numerically the validity of this hybrid modelling through comparisons with the original full kinetic model in two dimensions of the phase space. In this simplified context, we also study the dispersion relations of the two models (full kinetic and hybrid) and detail the pros and cons of two time integrators, namely the Hamiltonian splitting (inspired by the Hamiltonian structure of the hybrid model) and the Lawson methods (motivated by the linearization of the fluid part of the hybrid model). These two integrators are combined with adaptive time stepping strategies which ensure that the local error is lower than a user-specified tolerance for the whole simulation. Then, we extend these time integrators to a four dimensional framework in which wave propagation is parallel to a uniform external magnetic field, as in [1]. In this case, Hamiltonian splitting methods turn out to be less competitive than Lawson methods.

A Poisson bracket

In this Appendix, we prove that the bracket (7) is indeed a Poisson bracket. As usual, the linearity and skew-symmetry properties are easy to check. We then focus on the Jacobi identity. The bracket (7) can be reformulated as follows,

$$\{\mathcal{F},\mathcal{G}\} =: \{\mathcal{F},\mathcal{G}\}_{\mathrm{VM}} + \{\mathcal{F},\mathcal{G}\}_{jE}, \tag{55}$$

where the first bracket corresponds to the Vlasov-Maxwell bracket (see [34]) and the second part reads

$$\{\mathcal{F},\mathcal{G}\}_{jE} = \int_\Omega \Omega_{pe}^2 \left(\frac{\delta\mathcal{F}}{\delta\mathbf{j}_c}\cdot\frac{\delta\mathcal{G}}{\delta\mathbf{E}} - \frac{\delta\mathcal{G}}{\delta\mathbf{j}_c}\cdot\frac{\delta\mathcal{F}}{\delta\mathbf{E}}\right)\mathrm{d}\mathbf{x} + \int_\Omega \Omega_{pe}^2\mathbf{B}_0\cdot\left(\frac{\delta\mathcal{F}}{\delta\mathbf{j}_c}\times\frac{\delta\mathcal{G}}{\delta\mathbf{j}_c}\right)\mathrm{d}\mathbf{x}.$$

Using the above decomposition, the Jacobi identity can be written as follows,

$$\begin{aligned}
&\{\{\mathcal{F},\mathcal{G}\},\mathcal{H}\} + \{\{\mathcal{G},\mathcal{H}\},\mathcal{F}\} + \{\{\mathcal{H},\mathcal{F}\},\mathcal{G}\}\\
&= \{\{\mathcal{F},\mathcal{G}\}_{\mathrm{VM}},\mathcal{H}\}_{\mathrm{VM}} + \{\{\mathcal{F},\mathcal{G}\}_{\mathrm{VM}},\mathcal{H}\}_{jE},\\
&+ \{\{\mathcal{F},\mathcal{G}\}_{jE},\mathcal{H}\}_{\mathrm{VM}} + \{\{\mathcal{F},\mathcal{G}\}_{jE},\mathcal{H}\}_{jE} + \mathrm{cyc},
\end{aligned} \tag{56}$$

where $\mathcal{F},\mathcal{G},\mathcal{H}$ are functionals of the unknown and cyc is used to denote cyclic permutation. From the bracket theorem in [35], we only need to consider the functional derivatives of $\{\mathcal{F},\mathcal{G}\}$ modulo the second derivative terms, which, with abuse of notations, gives

$$\begin{aligned}
&\frac{\delta\{\mathcal{F},\mathcal{G}\}_{\mathrm{VM}}}{\delta\mathbf{j}_c} = \mathbf{0}, \quad \frac{\delta\{\mathcal{F},\mathcal{G}\}_{\mathrm{VM}}}{\delta\mathbf{E}} = \mathbf{0},\\
&\frac{\delta\{\mathcal{F},\mathcal{G}\}_{jE}}{\delta f_h} = 0, \quad \frac{\delta\{\mathcal{F},\mathcal{G}\}_{jE}}{\delta\mathbf{E}} = \mathbf{0}, \quad \frac{\delta\{\mathcal{F},\mathcal{G}\}_{jE}}{\delta\mathbf{B}} = \mathbf{0}.
\end{aligned} \tag{57}$$

So the second term and third term in (56) are all zeros. As $\frac{\delta\{\mathcal{F},\mathcal{G}\}_{jE}}{\delta\mathbf{E}}=\mathbf{0}$, and $\frac{\delta\{\mathcal{F},\mathcal{G}\}_{jE}}{\delta\mathbf{j}_c}=\mathbf{0}$ (in the sense of modulo the second variational derivatives), we know that the fourth term in (56) is zero.

Next only the first term in (56) is left. The starting point is the classical Poisson bracket of Vlasov–Maxwell equations,

$$\begin{aligned}\{\bar{\mathcal{F}},\bar{\mathcal{G}}\}[f_h,\mathbf{E},\bar{\mathbf{B}}] = &= \int_\Omega\int_{\mathbb{R}^3} f_h\Big[\frac{\delta\bar{\mathcal{F}}}{\delta f_h},\frac{\delta\bar{\mathcal{G}}}{\delta f_h}\Big]_{xv}\mathrm{d}\mathbf{v}\mathrm{d}\mathbf{x}\\ &+\int_\Omega\int_{\mathbb{R}^3} f_h\left(\nabla_{\mathbf{v}}\frac{\delta\bar{\mathcal{F}}}{\delta f_h}\cdot\frac{\delta\bar{\mathcal{G}}}{\delta\mathbf{E}}-\nabla_{\mathbf{v}}\frac{\delta\bar{\mathcal{G}}}{\delta f_h}\cdot\frac{\delta\bar{\mathcal{F}}}{\delta\mathbf{E}}\right)\mathrm{d}\mathbf{v}\mathrm{d}\mathbf{x}\\ &+\int_\Omega\int_{\mathbb{R}^3} f_h\bar{\mathbf{B}}\left(\nabla_{\mathbf{v}}\frac{\delta\bar{\mathcal{F}}}{\delta f_h}\times\nabla_{\mathbf{v}}\frac{\delta\bar{\mathcal{G}}}{\delta f_h}\right)\mathrm{d}\mathbf{v}\mathrm{d}\mathbf{x}\\ &+\int_\Omega\left(\nabla\times\frac{\delta\bar{\mathcal{F}}}{\delta\mathbf{E}}\cdot\frac{\delta\bar{\mathcal{G}}}{\delta\bar{\mathbf{B}}}-\nabla\times\frac{\delta\bar{\mathcal{G}}}{\delta\mathbf{E}}\cdot\frac{\delta\bar{\mathcal{F}}}{\delta\bar{\mathbf{B}}}\right)\mathrm{d}\mathbf{x},\end{aligned}\tag{58}$$

where we used the coordinate transformation $\bar{\mathbf{B}}=\mathbf{B}-\mathbf{B}_0$ and we introduced the functional $\bar{\mathcal{F}}[f_h,\mathbf{E},\bar{\mathbf{B}}]$ as

$$\bar{\mathcal{F}}[f_h,\mathbf{E},\bar{\mathbf{B}}]=\mathcal{F}[f_h,\mathbf{E},\bar{\mathbf{B}}-\bar{\mathbf{B}}_0]=\mathcal{F}[f_h,\mathbf{E},\mathbf{B}].$$

We have the following relations of variational derivatives,

$$\frac{\delta\bar{\mathcal{F}}}{\delta f_h}=\frac{\delta\mathcal{F}}{\delta f_h},\quad \frac{\delta\bar{\mathcal{F}}}{\delta\mathbf{E}}=\frac{\delta\mathcal{F}}{\delta\mathbf{E}},\quad \frac{\delta\bar{\mathcal{F}}}{\delta\bar{\mathbf{B}}}=\frac{\delta\mathcal{F}}{\delta\mathbf{B}}.\tag{59}$$

Substituting the above variational derivatives into (58), we have

$$\begin{aligned}\{\bar{\mathcal{F}},\bar{\mathcal{G}}\}[f_h,\mathbf{E},\bar{\mathbf{B}}] &= \int_\Omega\int_{\mathbb{R}^3} f_h\Big[\frac{\delta\mathcal{F}}{\delta f_h},\frac{\delta\mathcal{G}}{\delta f_h}\Big]_{xv}\mathrm{d}\mathbf{v}\mathrm{d}\mathbf{x}\\ &+\int_\Omega\int_{\mathbb{R}^3} f_h\left(\nabla_{\mathbf{v}}\frac{\delta\mathcal{F}}{\delta f_h}\cdot\frac{\delta\mathcal{G}}{\delta\mathbf{E}}-\nabla_{\mathbf{v}}\frac{\delta\mathcal{G}}{\delta f_h}\cdot\frac{\delta\mathcal{F}}{\delta\mathbf{E}}\right)\mathrm{d}\mathbf{v}\mathrm{d}\mathbf{x}\\ &+\int_\Omega\int_{\mathbb{R}^3} f_h\left(\mathbf{B}+\mathbf{B}_0\right)\left(\nabla_{\mathbf{v}}\frac{\delta\mathcal{F}}{\delta f_h}\times\nabla_{\mathbf{v}}\frac{\delta\mathcal{G}}{\delta f_h}\right)\mathrm{d}\mathbf{v}\mathrm{d}\mathbf{x}\\ &+\int_\Omega\left(\nabla\times\frac{\delta\mathcal{F}}{\delta\mathbf{E}}\cdot\frac{\delta\mathcal{G}}{\delta\mathbf{B}}-\nabla\times\frac{\delta\mathcal{G}}{\delta\mathbf{E}}\cdot\frac{\delta\mathcal{F}}{\delta\mathbf{B}}\right)\mathrm{d}\mathbf{x}\\ &=:\{\mathcal{F},\mathcal{G}\}(f_h,\mathbf{E},\mathbf{B}).\end{aligned}\tag{60}$$

Then we know that the 'first term + cyc = 0' in (56), i.e., $\{\{\mathcal{F},\mathcal{G}\}_{\mathrm{VM}},\mathcal{H}\}_{\mathrm{VM}}+\mathrm{cyc}=0$, which ends the proof of the Jacobi identity (58).

B Dimensionless procedure

In Table 5, we introduce the physical parameters used for the dimensionless procedure (with e the elementary charge: $q_e=-e$). Moreover, we assume $\frac{\Omega_{pe}^2}{\Omega_{ce}^2}\frac{\bar{u}_c}{c}=1$ and $\frac{\Omega_{pe}^2}{\Omega_{ce}^2}\frac{\bar{u}_h}{c}\frac{\rho_h^{(0)}}{\rho_c^{(0)}}=$

Parameter	Value
t	$1/\lvert\Omega_{ce}\rvert$
x	$c/\lvert\Omega_{ce}\rvert$
v	c
B	$\lvert\Omega_{ce}\rvert m_e/e$
E	$c\lvert\Omega_{ce}\rvert m_e/e$
j_c	$e\rho_c^{(0)}\bar{u}_c$
$\int_{\mathbb{R}^3}\mathbf{v}f_h\,\mathrm{d}\mathbf{v}$	$\rho_h^{(0)}\bar{u}_h$

Table 5: Dimensionless system for the four dimensional hybrid model.

1 so that we get

$$\frac{\partial \mathbf{j}_c}{\partial t} = \bar{\Omega}_{pe}^2\mathbf{E} - \mathbf{j}_c \times \mathbf{B}_0, \tag{61}$$

$$\frac{\partial f_h}{\partial t} + \mathbf{v}\cdot\nabla f_h - (\mathbf{E} + \mathbf{v}\times(\mathbf{B}+\mathbf{B}_0))\cdot\nabla_{\mathbf{v}} f_h = 0, \tag{62}$$

$$\frac{\partial \mathbf{B}}{\partial t} = -\nabla\times\mathbf{E}, \tag{63}$$

$$\frac{\partial \mathbf{E}}{\partial t} = \nabla\times\mathbf{B} - \mathbf{j}_c + \int_{\mathbb{R}^3}\mathbf{v}f_h\mathrm{d}\mathbf{v}, \tag{64}$$

where $\bar{\Omega}_{pe}^2 = \frac{\Omega_{pe}^2}{\Omega_{ce}^2}$ denotes the dimensionless plasma frequency (which is denoted Ω_{pe}^2 in the paper).

C Dimensionless procedure for the $1dx - 1dv$ case

In Table 6, we introduce the physical parameters used for the dimensionless procedure of the hybrid system (2)-(5) in one dimension in space and velocity. Moreover, assuming $\frac{\rho_h^{(0)}}{\rho_c^{(0)}}\frac{\bar{u}_h}{\bar{u}_c} = 1$, we obtain (17).

Parameter	Value
t	$1/\Omega_{pe}$
x	$\bar{u}_c/\Omega_{pe}$
v	$\bar{u}_c$
E	$\Omega_{pe}m_e\bar{u}_c/q_e$
j_c	$q_e\rho_c^{(0)}\bar{u}_c$
$\int_{\mathbb{R}} v f_h\,\mathrm{d}v$	$\rho_h^{(0)}\bar{u}_h$

Table 6: Dimensionless system for the two dimensional hybrid model.

Acknowledgement

This work has been carried out within the framework of the EUROfusion Consortium and has received funding from the Euratom research and training programme 2014- 2018 and 2019-2020 under grant agreement No 633053. The views and opinions expressed herein do not necessarily reflect those of the European Commission. The work has been supported by the French Federation for Magnetic Fusion Studies (FR-FCM).

References

[1] F. Holderied, S. Possanner, A. Ratnani, and X. Wang, "Structure-preserving vs. standard particle-in-cell methods: The case of an electron hybrid model," *Journal of Computational Physics*, vol. 402, 2020.

[2] L. Chen and F. Zonca, "Physics of alfvén waves and energetic particles in burning plasmas," *Rev. Mod. Phys.*, vol. 88, p. 015008, 2016.

[3] Y. Katoh and Y. Omura, "Computer simulation of chorus wave generation in the earth's inner magnetosphere," *Geophysical Research Letters*, vol. 34, no. 3, 2007.

[4] X. Tao, "A numerical study of chorus generation and the related variation of wave intensity using the dawn code," *Journal of Geophysical Research: Space Physics*, 2014.

[5] C. Tronci, "Hamiltonian approach to hybrid plasma models," *Journal of Physics A: Mathematical and Theoretical*, vol. 43, no. 37, p. 375501, 2010.

[6] C. Tronci, E. Tassi, E. Camporeale, and P. J. Morrison, "Hybrid Vlasov–MHD models: Hamiltonian vs. non-hamiltonian," *Plasma Physics and Controlled Fusion*, vol. 56, no. 9, p. 095008, 2014.

[7] Y. Cheng, A. Christlieb, and X. Zhong, "Numerical study of the two-species vlasov-ampère system: Energy-conserving schemes and the current-driven ion-acoustic instability," *J. Comput. Phys.*, vol. 288, pp. 66–85, 2014.

[8] P. J. Morrison, "Structure and structure-preserving algorithms for plasma physics," *Physics of Plasmas*, vol. 24, no. 5, p. 055502, 2017.

[9] Y. Li, Y. He, Y. Sun, J. Niesen, H. Qin, and J. Liu, "Solving the Vlasov–Maxwell equations using hamiltonian splitting," *Journal of Computational Physics*, no. 396, 2019.

[10] Y. Li, N. Crouseilles, and Y. Sun, "Numerical simulations of Vlasov–Maxwell equations for laser plasmas based on Poisson structure," *Journal of Computational Physics*, vol. 405, 2020.

[11] M. Kraus, K. Kormann, P. J. Morrison, and E. Sonnendrücker, "GEMPIC: geometric electromagnetic particle-in-cell methods," *Journal of Plasma Physics*, vol. 83, no. 4, p. 905830401, 2017.

[12] N. Crouseilles, L. Einkemmer, and E. Faou, "Hamiltonian splitting for the Vlasov–Maxwell equations," *Journal of Computational Physics*, vol. 283, pp. 224–240, 2015.

[13] E. Hairer, *Geometric numerical integration : structure-preserving algorithms for ordinary differential equations*. Berlin New York: Springer, 2006.

[14] F. Casas, N. Crouseilles, E. Faou, and M. Mehrenberger, "High-order hamiltonian splitting for Vlasov-Poisson equations," *Numerische Mathematik*, vol. 135, no. 3, 2017.

[15] M. Hochbruck and A. Ostermann, "Exponential integrators," *Acta Numerica*, vol. 19, pp. 209–286, 2010.

[16] M. Hochbruck and A. Ostermann, "Explicit exponential Runge–Kutta methods for semilinear parabolic problems," *SIAM Journal on Numerical Analysis*, vol. 43, no. 3, pp. 1069–1090, 2005.

[17] J. D. Lawson, "Generalized Runge–Kutta processes for stable systems with large lipschitz constants," *SIAM Journal on Numerical Analysis*, vol. 4, no. 3, pp. 372–380, 1967.

[18] L. Isherwood, Z. J. Grant, and S. Gottlieb, "Strong stability preserving integrating factor Runge–Kutta methods," *Journal on Numerical Analysis*, vol. 56, no. 6, pp. 3276–3307, 2018.

[19] J. D. Lawson, "An order six Runge–Kutta process with extended region of stability," *Journal on Numerical Analysis*, 1967.

[20] N. Crouseilles, L. Einkemmer, and J. Massot, "Exponential methods for solving hyperbolic problems with application to collisionless kinetic equations," *Journal of Computational Physics*, no. 420, 2020.

[21] J. Dormand and P. Prince, "A family of embedded Runge–Kutta formulae," *Journal of Computational and Applied Mathematics*, vol. 6, no. 1, pp. 19 – 26, 1980.

[22] J. Dormand and P. Prince, "New Runge–Kutta algorithms for numerical simulation in dynamical astronomy," *Celestial mechanics*, no. 18, pp. 223–232, 1978.

[23] S. Balac and A. Fernandez, "Mathematical analysis of adaptive step-size techniques when solving the nonlinear Schrödinger equation for simulating light-wave propagation in optical fibers," *Optics Communications*, vol. 329, pp. 1–9, 2014.

[24] S. Balac and F. Mahé, "Embedded Runge–Kutta scheme for step-size control in the interaction picture method," *Computer Physics Communications*, vol. 184, no. 4, pp. 1211–1219, 2013.

[25] S. Blanes, F. Casas, and M. Thalhammer, "Splitting and composition methods with embedded error estimators," *Applied Numerical Mathematics*, vol. 146, pp. 400 – 415, 2019.

[26] E. Sonnendrücker, *Numerical Methods for the Vlasov–Maxwell equations*. Springer, 2015.

[27] B. D. Fried and S. D. Conte, *The Plasma Dispersion Function; the Hilbert transform of the Gaussian*. Academic Press, 1961.

[28] M. Suzuki, "Fractal decomposition of exponential operators with applications to many-body theories and Monte Carlo simulations," *Physics Letters A*, vol. 146, no. 6, pp. 319 – 323, 1990.

[29] G. Strang, "On the construction and comparison of difference schemes," *SIAM Journal on Numerical Analysis*, vol. 5, no. 3, pp. 506–517, 1968.

[30] F. Casas and A. Escorihuela-Tomàs, "Composition methods for dynamical systems separable into three parts," *Mathematics*, vol. 8, no. 4, 2020.

[31] J. Bernier and M. Mehrenberger, "Long-time behavior of second order linearized Vlasov–Poisson equations near a homogeneous equilibrium," *Kinetic Related Models*, no. 13, pp. 129–168, 2020.

[32] K. Korman and E. Sonnendrücker, "Energy-conserving time propagation for a structure-preserving particle-in-cell Vlasov–Maxwell solver," *Journal of Computational Physics*, no. 425, p. 109890, 2020.

[33] K. Korman, K. Reuter, and M. Rampp, "A massively parallel semi-lagrangian solver for the six-dimensional Vlasov–Poisson equation," *The International Journal of High Performance Computing Applications*, no. 425, pp. 924–947, 2019.

[34] J. E. Marsden and A. Weinstein, "The hamiltonian structure of the Maxwell–Vlasov equations," *Physica D: Nonlinear Phenomena*, no. 4, 1982.

[35] P. J. Morrison, "A general theory for gauge-free lifting," *Physics of Plasmas*, no. 20, 2013.